Comparing amyloid-β plaque burden with antemortem PiB PET in autosomal dominant and late-onset Alzheimer disease

Authors

Charles D. Chen[1], Nelly Joseph-Mathurin[1*], Namita Sinha[2,3*], Aihong Zhou[4*], Yan Li[5], Karl Friedrichsen[6], Austin McCullough[1], Erin E. Franklin[2], Russ Hornbeck[1], Brian Gordon[1], Vijay Sharma[1], Carlos Cruchaga[7], Alison Goate[8], Celeste Karch[7], Eric McDade[5], Chengjie Xiong[5], Randall J. Bateman[5], Bernardino Ghetti[9], John M. Ringman[10], Jasmeer Chhatwal[11], Colin L. Masters[12], Catriona McLean[13], Tammaryn Lashley[14,15], Yi Su[16,17], Robert Koeppe[18], Clifford Jack[19], William Klunk[20], John C. Morris[5], Richard J. Perrin[2,5], Nigel J. Cairns[2,5,21#], Tammie L.S. Benzinger[1#]

Affiliations

[1]Mallinckrodt Institute of Radiology, Washington University in St. Louis, St. Louis, MO, USA

[2]Department of Pathology and Immunology, Washington University in St. Louis, St. Louis, MO, USA

[3]Department of Pathology, University of Manitoba, Shared Health, Winnipeg, MB, Canada

[4]Department of Neurology, Xuanwu Hospital, Capital Medical University, Beijing, China

[5]Department of Neurology, Washington University in St. Louis, St. Louis, MO, USA

[6]Department of Ophthalmology and Visual Sciences, Washington University in St. Louis, St. Louis, MO, USA

[7]Department of Psychiatry, Washington University in St. Louis, St. Louis, MO, USA

[8]Department of Genetics and Genomic Sciences, Ichan School of Medicine at Mount Sinai, New York, NY, USA

[9]Department of Pathology and Laboratory Medicine, Indiana University School of Medicine, Indianapolis, IN, USA

[10]Department of Neurology, Keck School of Medicine of USC, Los Angeles, CA, USA

[11]Department of Neurology, Massachusetts General Hospital, Harvard Medical School, Boston, MA, USA

[12]The Florey Institute of Neuroscience and Mental Health, The University of Melbourne, VIC, Australia

[13]Department of Anatomic Pathology, Alfred Hospital, Melbourne, Australia

[14]UCL Queen Square Institute of Neurology, University College London, London, UK

[15]Queen Square Brain Bank for Neurological Disorders, University College London, London, UK

[16]Banner Alzheimer's Institute, Banner Health, Phoenix, AZ, USA

[17]Arizona Alzheimer's Consortium, Banner Health, Phoenix, AZ, USA

[18]Department of Radiology, University of Michigan, Ann Arbor, MI, USA

[19]Department of Radiology, Mayo Clinic, Rochester, MN, USA

[20]Department of Psychiatry, University of Pittsburgh, Pittsburgh, PA

[21]College of Medicine and Health, University of Exeter, Exeter, UK

[*]These authors contributed equally

[#]These authors are co-senior authors

Corresponding author

Tammie L.S. Benzinger

Email: benzingert@wustl.edu

Phone: (314) 362-1558

Fax: (314) 362-6110

Abstract

Pittsburgh compound B (PiB) radiotracer for positron emission tomography (PET) imaging can bind to different types of amyloid-β plaques and blood vessels (cerebral amyloid angiopathy). However, the relative contributions of different plaque subtypes (diffuse versus cored/compact) to *in vivo* PiB PET signal on a region-by-region basis is incompletely understood. Of particular interest is whether the same staging schemes for summarizing amyloid-β burden are appropriate for both late-onset and autosomal dominant forms of Alzheimer disease (LOAD and ADAD). Here we compared antemortem PiB PET with follow-up postmortem estimation of amyloid-β burden using stereologic methods to estimate the relative area fraction of diffuse and cored/compact amyloid-β plaques across 16 brain regions in 15 individuals with ADAD and 14 individuals with LOAD. In ADAD, we found that PiB PET correlated with diffuse plaques in the frontal, parietal, temporal, and striatal regions commonly used to summarize amyloid-β burden in PiB PET, and correlated with both diffuse and cored/compact plaques in the occipital lobe and parahippocampal gyrus. In LOAD, we found that PiB PET correlated with both diffuse and cored/compact plaques in the anterior cingulate, frontal lobe (middle frontal gyrus), and parietal lobe, and showed additional correlations with diffuse plaque in the amygdala and occipital lobe, and with cored/compact plaque in the temporal lobe. Thus, commonly used PiB PET summary regions predominantly reflect diffuse plaque burden in ADAD and a mixture of diffuse and cored/compact plaque burden in LOAD. In direct comparisons of ADAD and LOAD, postmortem stereology identified much greater mean amyloid-β plaque burdens in ADAD versus LOAD across almost all brain regions studied. However, standard PiB PET did not recapitulate these stereologic findings, likely due to non-trivial amyloid-β plaque burdens in ADAD within the cerebellum and brainstem – commonly used reference regions in PiB PET. Our findings suggest that PiB PET summary

regions correlate with amyloid-β plaque burden in both ADAD and LOAD; however, they might not be reliable in direct comparisons of regional amyloid-β plaque burden between the two forms of AD.

Keywords

Alzheimer disease, amyloid-β plaques, PiB PET, stereology

Introduction

Pittsburgh compound B (PiB) positron emission tomography (PET) is a powerful diagnostic tool that enables *in vivo* imaging of insoluble amyloid-β throughout the human brain at near-millimeter resolution [36]. This offers an opportunity to detect and monitor changes in amyloid-β plaque deposition during the course of Alzheimer disease (AD) clinical trials. However, some important characteristics of PiB, as it is applied *in vivo,* remain incompletely understood. Although PiB is known to bind to amyloid-β peptides associated with both diffuse and amyloid-β cored/compact plaques [43], the relative contributions of these plaque subtypes to *in vivo* PiB PET signal on a region-by-region basis remains incompletely understood. The distinction is of interest from a clinicopathological perspective, as cored/compact plaques are more likely than their diffuse counterparts to be neuritic [16, 40, 51]. Nonetheless, diffuse plaques are associated with deleterious effects on cognitive performance and are unlikely to be benign [55]. Additionally, as AD clinical trials involve both late-onset AD (LOAD) and autosomal dominant AD (ADAD) populations, there is a need to understand whether the staging schemes for summarizing amyloid-β burden in the former are appropriate for investigating the severity of β-amyloidosis in the latter. In contrast to individuals with LOAD, those with ADAD carry a mutation in one of three genes – *APP*, *PSEN1*, or *PSEN2* – and develop AD with a relatively predictable time of clinical onset. This defining characteristic of ADAD allows investigators to assess the extent to which candidate drugs

are preventing or delaying the onset of AD dementia, but this underlying difference in disease etiology may also lead to differences in the characteristics of β-amyloidosis between LOAD and ADAD populations [1, 57].

Commonly, postmortem staging of amyloid-β deposition in AD involves assessment of Thal phase [69] and the Consortium to Establish a Registry for Alzheimer disease (CERAD) neuritic plaque score [47], which have recently been incorporated, along with Braak neurofibrillary tangle (NFT) stage [4], into the ABC score [28]. Although very useful for some purposes, these systems only describe the general anatomic pattern of amyloid-β plaque deposition within the central nervous system (Thal phase) and the semi-quantitative maximal density of neuritic plaques within a prescribed, limited set of cortical regions (CERAD). For antemortem staging of amyloid-β deposition in AD, a volume of interest comprised of frontal, parietal, temporal, and striatal regions is typically constructed to focus on brain regions of greater relevance to AD disease pathology [37, 64]; however, these regions were derived by comparing groups of healthy individuals and individuals with LOAD. Thus, from both neuropathologic and imaging perspectives, it is unclear whether these staging schemes for amyloid-β burden are equally applicable to both ADAD and LOAD.

Therefore, to investigate more fully the qualities of β-amyloidosis in these two forms of AD, we examined two cohorts, representing ADAD and LOAD, using antemortem PiB PET imaging and unbiased stereologic methods to quantify postmortem amyloid-β burden contributed by diffuse and cored/compact plaques in 16 brain regions of interest, including seven summary regions typically of interest in PiB PET imaging of AD (frontal, parietal, and temporal lobes, anterior and posterior regions of the cingulate gyrus, caudate, and putamen), seven other regions typically of interest for the evaluation of various other AD and non-AD pathologic features

(occipital lobe, amygdala, hippocampus, parahippocampal gyrus, entorhinal cortex, globus pallidus, and thalamus), and two reference regions typically of interest in PiB PET imaging of AD (cerebellum and brainstem). We then compared these findings to corresponding antemortem PiB PET, to determine whether the relationship between histologic and PET assessments of amyloid-β pathology is influenced by plaque type, anatomic region, and form of AD. This study provides insights into the extent to which plaque subtypes are represented in typical PiB PET neuroimaging and the extent to which differences in amyloid-β plaque burden between ADAD and LOAD are represented in typical PiB PET. Thus, this study informs how PiB PET might best be applied to evaluate ADAD progression in AD clinical trials, and how amyloid-β clearance might be appropriately monitored in anti-amyloid-β drug trials.

Materials and methods

Cohort demographics

Participants selected for this histological/radiological comparison study were either enrolled in the Dominantly Inherited Alzheimer Network Observational Study (DIAN-Obs, *n*=14) or in longitudinal observational studies of the Charles F. and Joanne Knight Alzheimer Disease Research Center (Knight ADRC, *n*=15). One participant was enrolled in studies of the Knight ADRC, but had an ADAD mutation; this individual was grouped with participants from the DIAN-Obs to form the ADAD cohort (*n*=15), and the remaining participants from the Knight ADRC formed the LOAD cohort (*n*=14) in the current study (Table 1). All participants met the inclusion criteria, having undergone PiB PET prior to death, and having *high* AD neuropathologic change (ADNC) upon subsequent postmortem examination [48]. Cohort demographics are reported in Table 1.

To address other questions about PiB PET amyloid staging, a separate extended imaging cohort of 317 DIAN-Obs participants and 734 Knight ADRC participants was selected. These participants met the inclusion criteria of having had a clinical and cognitive assessment within 18 months of a PiB PET scan. Extended imaging cohort demographics are reported in Table 3. Protocols for the study have received prior approval by the local Institutional Review Board (IRB) or Ethics Committee of each DIAN site, and by the Washington University IRB for the Knight ADRC. Participants or their caregivers provided written informed consent.

Postmortem neuropathology

Neuropathologic assessment of cases included a systematic evaluation of histologic slides representing 16 areas from the left hemibrain by experienced neuropathologists (authors R.J.P. and N.J.C.) [7]. Following an established protocol, each left hemibrain was sliced after formalin fixation. The supratentorial portion of the cerebral hemisphere was sliced in the coronal plane; the cerebellum, parasagitally; and the brainstem, axially. Sixteen representative brain areas were sampled: the frontal lobe (middle frontal gyrus); temporal lobe (superior and middle temporal gyri); parietal lobe (inferior parietal cortex including the angular gyrus); occipital lobe (including the calcarine sulcus and parastriate cortex); anterior cingulate gyrus (at the level of the genu of the corpus callosum); posterior cingulate gyrus (including precuneus at the level of the splenium); amygdala; hippocampus, parahippocampal gyrus, and entorhinal cortex (at the level of the lateral geniculate nucleus); caudate, putamen, and globus pallidus (at the level of the anterior commissure); thalamus (including subthalamic nucleus); brainstem (midbrain, pons, medulla oblongata); and cerebellum (with the dentate nucleus). Slide-mounted six-micron-thick sections of formalin-fixed, paraffin-embedded tissue were stained with hematoxylin and eosin (H&E), with a modified Bielschowsky silver impregnation, and by immunohistochemistry (IHC) using

antibodies for amyloid-β (10D5, Eli Lilly, Indianapolis, IN, USA), phosphorylated tau (PHF-1, a gift from Dr. Peter Davies), phosphorylated alpha-synuclein (Cell Applications, San Diego, CA, USA), and phosphorylated TAR DNA binding protein of 43 kDa (TDP-43, Cosmo Bio USA, Carlsbad, CA, USA) to detect the histopathological hallmarks of AD as well as those of frequent comorbid pathologies (including non-AD tauopathies, TDP-43 proteinopathies, and α-synucleinopathies). The Area Fraction Fractionator probe in Stereo Investigator 10 (MBF Bioscience, Williston, VT, USA) was used to assess the burden of diffuse and cored/compact amyloid-β using stereologic methods as implemented in a computerized image analysis system. Plaque area fraction was assessed either in the gray matter of cortical gyri or subcortical nuclei. Diffuse amyloid-β plaques were identified by raters (A.Z. and N.S.) to be irregularly-shaped amyloid-β deposits, while cored/compact amyloid-β plaques were identified to be spherically-shaped amyloid-β deposits representing a dense central core (surrounded by a less compact halo of amyloid-β oligomers contributing to the diffuse rather than the compact amyloid-β plaque area fraction) [31, 73]. The degree of agreement among raters in assessing diffuse and cored/compact amyloid-β plaque burden was high (Cohen's κ>0.8). When assessing amyloid-β plaque area fraction, raters were blinded to any demographic information regarding the individuals who donated the tissue samples, as well as any information regarding their antemortem PiB PET acquisition.

Antemortem PiB PET imaging

Methods for antemortem PiB PET acquisition, performed in compliance with the DIAN protocol, have been described previously [2, 49]. Briefly, participants received an intravenous injection of approximately 15 mCi of [11C]PiB radiotracer [76]. PET images were attenuation compensated with the corresponding CT image, and reconstructed using the ordered subset expectation

maximization technique. Data from 40 to 70 minutes post injection were converted to regional standardized uptake value ratios (SUVRs) with the cerebellar gray matter as the standard reference region, with cerebellar white matter and brainstem evaluated as alternative reference regions in later analyses. Regional SUVRs of interest were defined by FreeSurfer [22] version 5.3 regions best corresponding to the areas sampled for neuropathology in a consensus between an experienced neuropathologist and radiologist (authors R.J.P. and T.L.S.B.) [10]. MR images used for FreeSurfer segmentation were also performed in compliance with the DIAN protocol, as described previously [2, 49]. Briefly, T1-weighted images (1.1 x 1.1 x 1.2 mm resolution) were acquired for all DIAN-Obs participants on 3T scanners within one year of their PET scan.

Methods for antemortem PiB PET and MRI at the Knight ADRC have been described previously [64, 65]. These methods notably differ from the DIAN protocol in the following manner: PET imaging data from the 30 to 60 minutes post injection were converted to regional SUVRs (in contrast to the 40-70 minute post-injection time window for DIAN) and MR imaging was acquired on either a 1.5 or 3T scanner (in contrast to only 3T scanners for DIAN).

Briefly, brain areas sampled for neuropathologic assessment were matched to FreeSurfer regions on the basis of shared nomenclature and spatial overlap on the left hemisphere (Online Resource 1). All data processing steps were performed using the PET Unified Pipeline [63, 64], a publicly-available software developed in house.

Statistical analysis

All statistical analyses were performed in R version 3.5.2 “Eggshell Igloo”. Multiple imputation was used in the ADAD (15 participants) and LOAD (14 participants) cohorts to estimate missing observations due to the occasional unavailability of postmortem tissue samples; specifically, 17 tissue samples in the ADAD cohort (out of a possible 240, yielding 7.1% missingness) and 13

tissue samples in the LOAD cohort (out of a possible 224, yielding 5.8% missingness) were unavailable and subsequently estimated by multiple imputation by chained equations using the predictive mean matching method and five imputations [6]. Pearson's *r* was used to measure the linear correlation between regional PiB PET SUVR and diffuse and compact plaque area fractions in ADAD and LOAD cohorts. *T*-values from Welch two sample *t*-tests were used to determine the extent to which regional PiB PET SUVR and diffuse and compact plaque area fractions differed between ADAD and LOAD cohorts. Area under the receiver operating characteristic curves (AUCs, interpreted as the probability that a randomly selected ADAD/LOAD individual has a higher regional PiB PET SUVR than a randomly selected non-carrier/young healthy control) were used to determine which regions were most frequently elevated in ADAD/LOAD versus young healthy controls. Hierarchical agglomerative clustering was used to visualize similarities in regional PiB PET SUVR distributions across participants (complete-linkage clustering using a Euclidean distance metric). All test statistics are accompanied by *p*-values adjusted for false discovery rate (FDR) control by the Benjamini-Hochberg procedure. A FDR of q=0.05 was chosen for discussion purposes, but all FDR-adjusted *p*-values have been reported for transparency [19].

Results

Cohort demographics

Participants who formed the ADAD cohort in this study (n=15) were mostly known *PSEN1* mutation carriers (n=13), male (n=9), lacking the *APOE4* allele (n=10), and died at the average age of 47 from AD with other co-morbidities (Table 1). All ADAD participants were Thal phase 5, and Braak NFT stage VI, with "frequent" CERAD neuritic plaque scores.

Participants who formed the LOAD cohort in this study (n=14) were mostly male (n=9) *APOE4* carriers (n=10) who died at the average age of 83 with AD and other co-morbidities.

LOAD participants were largely Thal phase 5 (with two borderline Thal phase 4/5 cases), Braak NFT stage V (*n*=10), with "frequent" CERAD neuritic plaque scores.

In addition to the age of death, the major difference to note between the ADAD and LOAD cohorts is that the imaging-autopsy interval in the ADAD cohort is on average less than the imaging-autopsy interval in the LOAD cohort (an average of 2.4 years versus an average of 4.7 years) due to procedural differences between DIAN-Obs and Knight ADRC studies. We address the potential impact of this difference in the Discussion.

In the extended imaging cohort, ADAD participants (*n*=317) were mostly *PSEN1* mutation carriers (*n*=131) or non-carriers/young healthy controls (*n*=133), female (*n*=182), and cognitively normal (*n*=251), lacked the *APOE4* allele (*n*=222), and underwent PiB PET at an average age of 38 (Table 3).

LOAD participants (*n*=734) were mostly female (*n*=421) and cognitively normal (*n*=615), lacked the *APOE4* allele (*n*=451), and underwent PiB PET at an average age of 69.

Correlations between PiB PET and stereologic measurements

Regional correlations between PiB PET SUVR and diffuse and compact plaque area fractions in the ADAD and LOAD cohorts are shown in Table 2. In the ADAD cohort, PiB PET SUVR was significantly correlated (FDR-adjusted p-value<0.05) with diffuse plaque burden in all PiB PET summary regions except for the putamen, and with both diffuse and cored/compact plaque burden in the occipital lobe and parahippocampal gyrus (reference regions were not assessed in these correlational analyses). In the LOAD cohort, PiB PET SUVR was significantly correlated with both diffuse and cored/compact plaque burdens in the anterior cingulate, frontal lobe, and parietal lobe summary regions, and with cored/compact plaque burden in the temporal lobe summary

region. Additionally, PiB PET SUVR was significantly correlated with diffuse plaque burden in the amygdala and occipital lobe.

Differences between ADAD and LOAD as measured by PiB PET and stereology

Regional differences in amyloid-β burden (as measured by PiB PET and stereology) between the ADAD and LOAD cohorts are shown in Fig. 1. Diffuse plaque burden was significantly greater in ADAD versus LOAD in all summary regions except for the parietal lobe, and in all other regions, except for the globus pallidus. Cored/compact plaque burden was also greater in ADAD versus LOAD, though only in the cerebellum and brainstem was this difference significant.

In contrast to stereologic measurements, PiB PET SUVRs (when calculated using the cerebellar gray matter as a reference region) showed no significant differences between ADAD versus LOAD in any summary region examined, with the exceptions of the caudate and the putamen. Additionally, PiB PET SUVR was significantly greater in ADAD versus LOAD in the hippocampus, occipital lobe, and thalamus. Alternative reference regions such as the brainstem, cerebellar white matter, and a combined cerebellar gray and white matter region were also investigated (Fig. 2). The brainstem as a reference region yielded results similar to those when cerebellar gray matter was used as a reference region (and additionally showed significant differences in the globus pallidus). When cerebellar white matter was used as a reference region, PiB PET SUVRs showed additional significant differences between ADAD versus LOAD in the anterior cingulate, amygdala, entorhinal cortex, globus pallidus, brainstem, and cerebellum. Use of the combined cerebellar gray and white matter reference region mostly recapitulated the significant differences between ADAD versus LOAD as seen with the cerebellar white matter reference region, with the exception of the amygdala and entorhinal cortex. Nonetheless, no reference region assessed in this study revealed significant between-cohort differences in SUVR

in the frontal and temporal lobes, posterior cingulate, and parahippocampal gyrus in a manner concordant with our stereology results. Additionally, the alternative reference regions showed significant between-cohort differences in SUVR in the globus pallidus, which was not seen in stereology.

PiB PET staging in ADAD versus LOAD

Regional distributions of PiB PET SUVRs in ADAD versus LOAD are shown in Fig. 3. Regional AUC analyses showed that ADAD participants frequently demonstrate elevated PiB PET SUVRs compared to non-carriers/young healthy controls across all brain regions, with several medial temporal lobe regions being the least frequently elevated, namely the amygdala, hippocampus, and entorhinal cortex (Fig. 3a). In contrast, LOAD participants most frequently demonstrate elevated PiB PET SUVRs compared to non-carriers/young healthy controls across several temporal lobe regions, namely the middle temporal, inferior temporal, and fusiform cortices (Fig. 3b). In a hierarchical agglomerative clustering dendrogram of ADAD cases, caudate and putamen PiB PET SUVRs cluster with cortical SUVRs such as those of the occipital lobe, frontal lobe, and the anterior and posterior cingulate (Fig. 3c). In contrast, in LOAD, caudate and putamen SUVRs cluster with medial temporal lobe SUVRs such as those of the parahippocampal gyrus, entorhinal cortex, amygdala, and hippocampus rather than frontal and cingulate cortex SUVRs (Fig. 3d).

Discussion

Evidence suggests that the primary substrate for PiB retention (and likely that of all PET amyloid-β radiotracers) is fibrillar amyloid-β [38]. Fibrillar amyloid-β is present in both diffuse and cored/compact plaques – although the density is probably much greater in the latter [15]. Therefore, *in vivo* PiB retention cannot distinguish between diffuse and cored/compact deposits of fibrillar amyloid-β. However, the total PiB signal will be primarily driven by the most abundant

form of fibrillar amyloid-β, whether in diffuse or cored/compact plaques. To determine which form of plaque (diffuse or cored/compact) is most associated with the *in vivo* PiB PET signal, postmortem-to-*in vivo* correlative studies must be performed. In this study, we compared the correlation of *in vivo* PiB PET retention with postmortem analyses of diffuse and cored/compact plaques in ADAD and LOAD to determine the major contributor to the *in vivo* PiB PET signal in these different forms of AD. From correlational analyses, PiB PET SUVRs in AD summary regions appear to reflect predominantly diffuse plaque burden in ADAD, and a mixture of diffuse and cored/compact plaque burden in LOAD. Outside of these summary regions, PiB PET SUVRs seem to correlate with both diffuse and cored/cored compact plaque burden in the occipital lobe and parahippocampal gyrus in ADAD, and with diffuse plaque burden in the occipital lobe and amygdala in LOAD. These differences suggest that the two forms of AD may require different β-amyloidosis staging schemes to interpret findings from PiB PET. Furthermore, the greater variability of plaque burden observed among ADAD cases additionally suggests that a staging scheme for ADAD might require adjustment for other factors, such as, perhaps, genetic subtype. Nonetheless, some caution is warranted: the presence of cored/compact plaques in several of the aforementioned brain regions is a sign of advanced disease which, in turn, is associated with altered blood flow. Changes in blood flow associated with advanced AD may alter PiB pharmacokinetics and cause nonspecific retention in affected brain areas [3]; such pathophysiologic changes may be partly responsible for the above observations.

Postmortem stereologic measurements of diffuse and cored/compact plaque burden are significantly greater in ADAD versus LOAD across the brain, yet standard antemortem PiB PET in the same individuals captured significant differences mostly in subcortical regions (specifically the caudate, putamen, and thalamus, as well as the hippocampus and occipital lobe) when using

either the cerebellar gray matter or brainstem as reference regions. One possible explanation for the lack of significant differences in cortical amyloid-β between the two cohorts as measured by PiB PET is offered by our stereology results; the cerebellum and brainstem – both commonly used as reference regions in LOAD studies due to their relatively low PiB PET signal in LOAD cohorts – have non-trivial amyloid-β plaque burdens in the ADAD cohort. These circumstances would tend to depress regional PiB PET SUVRs in those ADAD cases with substantial cerebellar and/or brainstem amyloid-β deposits and, thus, selectively reduce the mean SUVR of the ADAD cohort, relative to that of the LOAD cohort. Importantly, this observation suggests that cerebellar gray matter and brainstem may not be appropriate reference regions for evaluating amyloid-β burden with PiB PET in many cases of ADAD. An alternative reference region such as the cerebellar white matter was also evaluated in this study, though using the cerebellar white matter as a reference region only showed additional significant differences in amyloid-β burden between ADAD and LOAD in the anterior cingulate, amygdala, entorhinal cortex, brainstem, cerebellum, and globus pallidus (though this last region did not demonstrate significantly different amyloid-β plaque burden in ADAD versus LOAD). Unfortunately, previous work has shown that white matter reference regions may exhibit confounding age-effects, especially in studies of LOAD [44]. Thus, comparing regional differences in amyloid-β burden accurately between ADAD and LOAD cohorts using PiB PET may be impossible using a standard approach. One compromise solution may be to use a combined cerebellar gray and white matter reference region, which mitigates the effects of amyloid-β burden in the cerebellar gray matter of ADAD individuals and potentially also the age-related changes in the cerebellar white matter of LOAD individuals; however, this combined reference region still fails to demonstrate the elusive between-cohort differences in

amyloid-β burden in several regions implicated by our stereology results (Fig. 2). Potential reasons for this discrepancy are noted in the penultimate paragraph of this Discussion.

Finally, our results suggest that diffuse and cored/compact amyloid-β plaque burdens are on average greater in ADAD than in LOAD, with diffuse plaque area fraction being greater in ADAD versus LOAD in all brain regions assessed in this study, except for the parietal lobe and globus pallidus. Interestingly, another neuropathological study showed a higher *density* of compact plaques and an equal degree of diffuse plaques in ADAD relative to LOAD, though this was a semi-quantitative study where regional distribution was not taken into account [57]. While overall amyloid-β plaque burdens may generally be greater in ADAD versus LOAD, this difference may not be true for each case of ADAD. Our current experiment encapsulates the heterogeneity in phenotypes previously described across the amyloid-β PET imaging literature of ADAD: Koivunen and colleagues found striatal elevations in specific *PSEN1* mutation carriers [41] and Remes and colleagues found striatal and posterior cingulate elevations in *APP* mutation carriers [56]; Theuns and colleagues found an *APP* mutation carrier who demonstrated elevated amyloid-β burden in cerebral cortex with sparing of subcortex and cerebellum [70]; Tomiyama and colleagues found an *APP* mutation carrier who demonstrated very low amyloid-β signal in the brain [72], and Schöll and colleagues found a similar result in another two *APP* mutation carriers [61]. Beyond imaging studies, many other studies have observed heterogeneities in the ADAD population, including in age of onset and clinical presentation [42, 59, 62, 66] as well as implicated amyloid-β species [46, 54]. It would be of future interest to determine how the heterogeneities observed in these other domains may relate to the heterogeneities we observed in postmortem stereology of diffuse and cored/compact plaque burden.

While general correspondence between amyloid-β PET and neuropathologic assessment has been evaluated by several studies, few have done so with unbiased, quantitative stereologic measurements as in the current study. In general, we found that the semi-quantitative ABC scoring of neuropathology cases using Thal phase, Braak NFT stage, and CERAD neuritic plaque score [29] was not granular enough to capture differences and variability between individuals and cohorts that were seen when using quantitative stereologic measurements. Notably, all ADAD cases in our study were Thal phase 5, Braak NFT stage VI, and CERAD neuritic plaque score "frequent". Additionally, LOAD cases were mostly Thal phase 5 (with two borderline exceptions), mostly Braak NFT stage V, and all CERAD neuritic plaque score "frequent". This is consistent with our previous study, which found substantial inter-cohort differences in tau neurofibrillary tangle, neuropil thread, and neuritic plaque burden in a cohort of seven ADAD and 10 LOAD individuals who were nonetheless all assessed as Braak NFT stage VI [10].

Nevertheless, several findings from previous studies are concordant with ours, even when reagents and analytic methods differ substantially. For example, Klunk and colleagues compared PiB PET SUVRs of two *PSEN1* mutation carriers who had developed clinical AD – using pons as the reference region – with qualitative assessment of 10D5-immunostained amyloid-β plaques in the striatum of the parent of one of the mutation carriers; from this indirect study, they found intense amyloid-β radiotracer binding in the striatum, consistent with findings from postmortem neuropathology [39]. Two caveats, however: first, the premise that motivated Klunk and colleagues to use the pons as a reference region – that the pons is a region free of amyloid-β – may not be true for all cases of ADAD; indeed, as our study illustrates, use of this reference region might account for their observation that cortical amyloid-β radiotracer retention was not greater in ADAD versus LOAD. Additionally, we cannot exclude the possibility that the distribution and

388 characteristics of amyloid-β deposits across individuals with the same pathogenic variant
389 completely align.

390 Imaging-pathology correspondence has not been well-studied in ADAD beyond the
391 previous paper, but it has been more extensively studied in the LOAD literature. Clark and
392 colleagues [12] compared semiquantitative visual ratings and [18F]AV45 (also known as
393 florbetapir or Amyvid) SUVRs with semiquantitative rating and quantitative – but not stereologic
394 – assessment of 4G8 immunostained amyloid-β plaques. This comparison was done across six
395 regions of interest in 29 individuals (which was expanded to 59 individuals in a follow-up study
396 [11]), ranging from cognitively normal to clinically diagnosed with LOAD and non-AD dementia,
397 but all approaching the end of life [12]. In accord with the current study, Clark and colleagues
398 found strong correlations between ante- and postmortem measurements of amyloid-β burden in
399 the frontal, parietal, and temporal lobes and anterior cingulate gyrus, though they additionally
400 found significant correlations in the posterior cingulate and precuneus, which did not reach
401 significance for LOAD in our current study. That our LOAD cohort did not include cognitively
402 normal or non-AD dementia individuals may have contributed to this difference between the two
403 studies; other potential factors include the use of different amyloid-β PET binding agents and
404 different primary anti amyloid-β antibodies.

405 Particularly of interest are LOAD imaging-pathology studies that also use the PiB PET
406 radioligand. Of note among these is a study by Ikonomovic and colleagues, which compared PiB
407 PET distribution volume ratios (DVRs) and quantitative – but not stereologic – assessment of 6-
408 CN-PiB stained and 6E10 immunostained amyloid-β plaques in a single LOAD individual across
409 19 regions of interest, including the cortical ribbon and most subcortical nuclei, all sampled in a
410 single axial plane; correlations were strong overall between regional PiB PET DVRs and 6E10

411 immunostained diffuse and cored/compact amyloid-β plaques [31]. Another study is by Driscoll
412 and colleagues, who investigated six older adults – none of whom progressed to certain AD
413 dementia – by comparing regional PiB PET DVRs with stereologic measurements of 6E10
414 immunostained amyloid-β plaques; they found statistically significant correlations in the anterior
415 and posterior regions of the cingulate gyrus and in the precuneus [18]. Murray and colleagues
416 investigated 35 cases with antemortem PiB PET imaging and postmortem semi-quantitative
417 scoring and found a PiB PET summary region SUVR of 1.4 was approximately equivalent to a
418 Thal phase of 1 to 2, and that Thal phase, but not Braak NFT stage or cerebral amyloid angiopathy
419 (CAA) score, predicted PiB PET summary region SUVRs [50]. Moving beyond PiB PET studies,
420 Curtis and colleagues investigated 68 patients with antemortem [18F]flutemetamol PET and
421 postmortem semi-quantitative scores; the authors found a median sensitivity and specificity of
422 88% among five visual readers interpreting [18F]flutemetamol PET scans as positive or negative,
423 compared to the reference standard of postmortem neuritic plaque density as assessed by the
424 modified CERAD score [14]. Ikonomovic and colleagues studied 106 end-of-life subjects with
425 antemortem [18F]flutemetamol PET and postmortem semi-quantitative scores, finding that the
426 probability of an abnormal [18F]flutemetamol PET scan increased with neocortical neuritic plaque
427 density (though diffuse plaques and CAA may explain cases with abnormal [18F]flutemetamol
428 PET scans but low neuritic plaque burden), and concluding that amyloid-β in the form of neuritic
429 plaques is the primary form of amyloid-β detectable by [18F]flutemetamol PET [30]. Sabri and
430 colleagues studied 74 trial participants with antemortem [18F]florbetaben PET and postmortem
431 CERAD scores and concluded that [18F]florbetaben PET demonstrated high sensitivity and
432 specificity for detecting neuritic plaques [60]. Thal and colleagues investigated three cohorts of
433 human autopsy cases neuropathologically and biochemically for the distribution of plaques and

CAA, quantity, and composition of amyloid-β pathology and found that these three measures correlated with each other and with [18F]flutemetamol PET, neurofibrillary tangles, neuritic plaques, and dementia severity [68].

This current study does have some limitations. One potential criticism of the current study is that the imaging-autopsy interval, namely the time interval between the antemortem PiB PET imaging visit and the start of autopsy, could not be matched between ADAD and LOAD cohorts. In the ADAD cohort, individuals continued to undergo PiB PET imaging exams well after showing clinical signs of AD, and imaging-autopsy intervals in the cohort ranged from 0.68 to 5.6 years with an average of 2.4 years. In contrast, individuals in the LOAD cohort did not undergo imaging studies once they progressed to moderate dementia, and the imaging-autopsy intervals ranged from 0.3 to 9.6 years with an average of 4.7 years. The primary concern would be whether this difference caused greater discordances between ante- and postmortem assessments of amyloid-β burden in the LOAD versus ADAD cohort. Relevant to this issue, two points of evidence suggest that this imaging-autopsy interval difference is not likely to account for all of the differences in amyloid burden between LOAD and ADAD. First, the strongest correlation between PiB PET SUVR and diffuse plaque burden in the entire study was observed within the LOAD cohort, within the parietal lobe (Pearson's r=0.83, FDR-adjusted p-value=0.00098). Second, according to highly-cited leading articles in the field of AD research, amyloid-β deposition in the brain occurs over decades, and the majority of it occurs well before clinical symptoms of AD appear [33, 74]; in this scenario, a difference of 2.4 years near the end of that 15-to-20-year period is unlikely to impact amyloid burdens substantively. Additionally, the *rate* of amyloid-β deposition slows as an individual enters the symptomatic phase of the disease, and this phenomenon lessens the effect of the imaging-autopsy interval on differences in plaque burden prior to and at death [32]. A related limitation to

457 the long interval between PiB PET and postmortem analysis is that the AD process also advanced
458 during this interval – the PET findings were in the milder stages of AD, whereas the postmortem
459 analysis was at the end-stage of the disease, so end-stage findings may not reflect mild stage
460 findings and vice-versa.

461 Another difference between the ADAD and LOAD cohorts to be mindful of is age. Age-
462 related co-morbidities are far more common in LOAD than in ADAD [7], and three LOAD
463 participants in this study were over 90 years of age. Specifically in our study, we observed both
464 microinfarcts and TDP-43 pathology, both of which are common co-morbidities among such
465 "oldest-old" individuals [13, 52]. Nonetheless, since the focus of the current study is the
466 quantification of amyloid-β burden, the presence of co-morbidities and their potential to contribute
467 to dementia do not complicate our main findings. This is particularly relevant as there are no
468 known reports of amyloid-β immunostain or radioligand off-target binding to microinfarcts or
469 TDP-43 aggregates, which would be one way these co-morbidities could complicate the
470 quantification of amyloid-β burden.

471 Another limitation of our study is the manner in which regions were matched between
472 imaging and neuropathology. Regional PiB PET SUVRs were derived from FreeSurfer regions
473 (from the Desikan-Killiany atlas [22]) whereas regional plaque area fractions were derived from
474 standard tissue blocks included in DIAN and Knight ADRC postmortem assessment protocols [7].
475 FreeSurfer regions and tissue blocks were matched on the basis of shared nomenclature or spatial
476 overlap; however, this solution is imperfect. One primary issue is that brain structures were
477 segmented in their entirety through imaging, but were only be sampled in a chosen plane in
478 neuropathology. For example, neuropathologic assessment of the hippocampus and
479 parahippocampal gyrus was performed at the level of the lateral geniculate nucleus, whereas the

hippocampus and parahippocampal gyrus were assessed in their entirety in imaging. Previous work has noted this may lead to discordances in imaging-neuropathology comparisons [10], and future work will aim to target the same regions across both imaging and neuropathology with greater accuracy using improved co-registration methods [20].

Another limitation is that our study does not account for the presence or degree of amyloid-β deposition in the walls of small cortical blood vessels, or CAA, during stereologic quantification. CAA is known to be an additional source of the PiB PET signal [9], potentially contributing to its regional variability across disease conditions [34, 45], and can be more prevalent and severe in ADAD relative to LOAD [57]. As such, it may account for higher PiB PET signal in the occipital lobe in ADAD versus LOAD independently of plaque burden, and otherwise influence the correlation between amyloid-β pathology and PiB PET signal in ways not measured in the current study. CAA may also impact PiB PET SUVR measurements more broadly by appearing within the cerebellum. Like the occipital lobe, the cerebellum often shows disproportionately high CAA relative to other brain areas. However, in the current study, when assessed semi-quantitatively [53, 75], CAA does not show any statistically significant correlations with diffuse or cored/compact plaque burden, or PiB PET SUVR, in either the ADAD or LOAD cohort.

We also acknowledge two other limitations of this study. The current imaging-neuropathology findings cannot address whether the PiB PET signal maintains the correlations with diffuse and compact plaque burden as seen here throughout the course of ADAD and LOAD. End-stage postmortem studies cannot determine the absolute staging of different plaque morphologies, though the earliest plaque forms observed in the non-demented aged brain are typically of the diffuse type. This observation may impact the appropriate time to administer anti-amyloid-β drug interventions, which would aim to prevent more cored/compact plaque formation;

cored/compact plaques, because they are more likely to be neuritic, may be more closely linked than diffuse plaques to tau pathology, neurodegeneration, and cognitive impairment. Nonetheless, findings from our extended imaging cohort support the idea of developing separate PET staging schemes for ADAD versus LOAD across the lifespan as well. In ADAD, we see most frequent elevations of amyloid-β burden in regions outside the medial temporal lobe, while in LOAD, we see most frequent elevations of amyloid-β burden in posterolateral temporal lobe regions, suggesting two different origins of β-amyloidosis in the two diseases. Furthermore, in ADAD, striatal amyloid-β accumulation appears in step with other cortical amyloid-β accumulation, whereas in LOAD, striatal amyloid-β accumulation appears along with medial temporal lobe amyloid-β accumulation. Our observations in the ADAD participants are consistent with prior longitudinal analyses in the ADAD population [24] and our observations in the LOAD participants are consistent with prior LOAD schemes, in particular, the scheme of Grothe and colleagues [26], who propose that amyloid-β deposition appears first in temporobasal and frontomedial regions, and appears latest in the medial temporal lobe and striatum. Additional work is needed to understand how changes in the spatial distribution and intensity of the PiB PET signal throughout the disease course of ADAD relates to the distribution of plaque pathology, which has been more extensively studied in the context of LOAD [26, 27, 35, 67].

Finally, we note that our current histological approach measures amyloid-β plaque burden in a semi-quantitative approach by its *area*. Thus, in a situation where a diffuse plaque and cored/compact plaque might have the same area, the cored/compact plaque may have a higher *mass* of amyloid-β. This is in contrast to the semi-quantitative nature of PiB PET, where PiB retention is proportional to the number of available binding sites – presumably determined by the *mass* of fibrillar amyloid-β – whether amyloid-β is deposited in the form of a diffuse or

cored/compact plaque. This presumption is also somewhat speculative as it is unknown whether the PiB radiotracer can fully penetrate a solid fibrillar plaque core within the typical timeframe of a PiB PET imaging study; it is also possible that conformational and/or biochemical differences might alter the availability of binding sites. The numerous aforementioned differences in how PiB PET and amyloid-β plaques are quantified leave room for future studies to develop more comparable semi-quantitative measures of ante- and postmortem amyloid-β burden. Two promising directions are light microscope high-resolution autoradiography [8], which might be able to quantify the intensity of radiotracer signal contributed by individual plaques in a manner that avoids the issue of quantifying the mass of fibrillar amyloid-β by its area; and single-molecule imaging [17] and small angle neutron scattering [5, 71], which may help us understand the relationship between fibrillar amyloid-β aggregates and various amyloid-β plaque types. A third approach would be to move away from purely neuropathological approaches of assessing characteristics of plaque pathology to instead focus on biochemical approaches. Biochemical approaches quantifying amyloid-β species from brain tissue homogenates have shed light on amyloid pathology in LOAD, indicating increased amounts of Aβ40 or Aβ42(43) relative to plaque types [23, 25]. More recently, a study in LOAD evaluated biochemical fractions of amyloid-β from brain tissue compared to PET imaging to estimate which biochemical pools were most affected in AD, and derived a first approximation of the rates of amyloid-β accumulation [58]. Such approaches can also reveal distinct molecular profiles of amyloid-β in LOAD and ADAD [21].

In summary, our data indicate that there is a close association between fibrillar amyloid-β burden as visualized by PiB PET and as assessed by postmortem stereologic measures. Caveats may be raised: individuals with ADAD show considerable variability in amyloid-β burden and distribution that can also differ considerably from that typical of LOAD; therefore, summary and

reference regions commonly used in PiB PET studies of LOAD may potentially need to be adjusted for PiB PET studies of ADAD. This point is especially important when evaluating anti-amyloid-β drug trials that enroll participants with ADAD. In such studies, investigators should be alert to the possibility of variable drug responses and interpret differences in cross-sectional measures of amyloid-β burden between treatment groups with care; indeed, individual-focused longitudinal monitoring strategies might be favorable. Additionally, when comparing trials of the same anti-amyloid-β drug conducted in ADAD versus LOAD, investigators should note that the choice of reference region can strongly influence interpretations of regional amyloid-β burden differences between cohorts.

Acknowledgements

Funding

Data collection and sharing for this project was supported by the Knight Alzheimer Disease Research Center (Knight ADRC, P30AG066444, P01AG026276, P01AG03991) and the Dominantly Inherited Alzheimer Network (DIAN, U19AG032438). This manuscript has been reviewed by DIAN Study investigators for scientific content and consistency of data interpretation with previous DIAN Study publications. We acknowledge the altruism of the participants and their families and contributions of the Knight ADRC and DIAN research and support staff at each of the participating sites for their contributions to this study. For the provision of brain tissue and staining, we acknowledge the Knight ADRC Neuropathology Core and the DIAN Neuropathology Core (P01AG003991). We thank the staff of the Betty Martz Laboratory for Neurodegenerative Disease for their excellent technical support. The authors also acknowledge support from the Neuroimaging Informatics and Analysis Center (P30NS098577). C.D.C. acknowledges support from the NSF GRFP (DGE-1745038). N.J-M. acknowledges support from the Alzheimer's

Association International Research Grant Program (AARFD-20-681815). B.A.G. acknowledges support from the NIH (K01AG053474). J.C.M. acknowledges support from the NIH (UF1AG032438).

Competing interests

J.C. has served on a medical advisory board for Otsuka Pharmaceuticals. J.C.M. is funded by NIH grants # P30 AG066444; P01AG003991; P01AG026276; U19 AG032438; and U19 AG024904. Neither J.C.M. nor his family owns stock or has equity interest (outside of mutual funds or other externally directed accounts) in any pharmaceutical or biotechnology company. T.L.S.B. has investigator-initiated research funding from the NIH, the Alzheimer's Association, the Barnes-Jewish Hospital Foundation and Avid Radiopharmaceuticals (a wholly owned subsidiary of Eli Lilly); participates as a site investigator in clinical trials sponsored by Avid Radiopharmaceuticals, Eli Lilly, Biogen, Eisai, Jaansen, and Roche; serves as an unpaid consultant to Eisai and Siemens; and is on the Speaker's Bureau for Biogen.

Data and materials availability

Data is available by request to the Knight ADRC (knightadrc.wustl.edu/research/resourcerequest.htm) and the DIAN-Obs (dian.wustl.edu/our-research/observational-study/dian-observational-study-investigator-resources/data-request-terms-and-instructions/).

References

1. Bateman RJ, Aisen PS, De Strooper B, Fox NC, Lemere CA, Ringman JM, Salloway S, Sperling RA, Windisch M, Xiong C (2011) Autosomal-dominant Alzheimer's disease: A review and proposal for the prevention of Alzheimer's disease. Alzheimer's Res. Ther. 2
2. Benzinger TLS, Blazey T, Jack CR, Koeppe RA, Su Y, Xiong C, Raichle ME, Snyder AZ,

Ances BM, Bateman RJ, Cairns NJ, Fagan AM, Goate A, Marcus DS, Aisen PS, Christensen JJ, Ercole L, Hornbeck RC, Farrar AM, Aldea P, Jasielec MS, Owen CJ, Xie X, Mayeux R, Brickman A, McDade E, Klunk W, Mathis CA, Ringman J, Thompson PM, Ghetti B, Saykin AJ, Sperling RA, Johnson KA, Salloway S, Correia S, Schofield PR, Masters CL, Rowe C, Villemagne VL, Martins R, Ourselin S, Rossor MN, Fox NC, Cash DM, Weiner MW, Holtzman DM, Buckles VD, Moulder K, Morris JC (2013) Regional variability of imaging biomarkers in autosomal dominant Alzheimer's disease. Proc Natl Acad Sci U S A 110:E4502–E4509. doi: 10.1073/pnas.1317918110

3. Van Berckel BNM, Ossenkoppele R, Tolboom N, Yaqub M, Foster-Dingley JC, Windhorst AD, Scheltens P, Lammertsma AA, Boellaard R (2013) Longitudinal amyloid imaging using 11C-PiB: Methodologic considerations. J Nucl Med 54:1570–1576. doi: 10.2967/jnumed.112.113654

4. Braak H, Braak E (1991) Neuropathological stageing of Alzheimer-related changes. Acta Neuropathol 82:239–259. doi: 10.1007/BF00308809

5. Burkoth TS, Benzinger TLS, Urban V, Lynn DG, Meredith SC, Thiyagarajan P (1999) Self-assembly of Aβ((10-35))-PEG block copolymer fibrils [13]. J. Am. Chem. Soc. 121:7429–7430

6. van Buuren S, Groothuis-Oudshoorn K (2011) mice: Multivariate imputation by chained equations in R. J Stat Softw 45:1–67. doi: 10.18637/jss.v045.i03

7. Cairns NJ, Perrin RJ, Franklin EE, Carter D, Vincent B, Xie M, Bateman RJ, Benzinger T, Friedrichsen K, Brooks WS, Halliday GM, McLean C, Ghetti B, Morris JC (2015) Neuropathologic assessment of participants in two multi-center longitudinal observational studies: The Alzheimer Disease Neuroimaging Initiative (ADNI) and the Dominantly

618 Inherited Alzheimer Network (DIAN). Neuropathology 35:390–400. doi:
619 10.1111/neup.12205
620 8. Caro LG (1964) Chapter 16 High-Resolution Autoradiography. Methods Cell Biol 1:327–
621 363. doi: 10.1016/S0091-679X(08)62098-1
622 9. Charidimou A, Farid K, Baron JC (2017) Amyloid-PET in sporadic cerebral amyloid
623 angiopathy. Neurology 89:1490–1498. doi: 10.1212/WNL.0000000000004539
624 10. Chen CD, Holden TR, Gordon BA, Franklin EE, Li Y, Coble DW, Luo H, Bateman RJ,
625 Ances BM, Perrin RJ, Benzinger TLS, Cairns NJ, Morris JC (2020) Ante- and
626 postmortem tau in autosomal dominant and late-onset Alzheimer's disease. Ann Clin
627 Transl Neurol 7:2475–2480. doi: 10.1002/acn3.51237
628 11. Clark CM, Pontecorvo MJ, Beach TG, Bedell BJ, Coleman RE, Doraiswamy PM, Fleisher
629 AS, Reiman EM, Sabbagh MN, Sadowsky CH, Schneider JA, Arora A, Carpenter AP,
630 Flitter ML, Joshi AD, Krautkramer MJ, Lu M, Mintun MA, Skovronsky DM (2012)
631 Cerebral PET with florbetapir compared with neuropathology at autopsy for detection of
632 neuritic amyloid-β plaques: A prospective cohort study. Lancet Neurol 11:669–678. doi:
633 10.1016/S1474-4422(12)70142-4
634 12. Clark CM, Schneider JA, Bedell BJ, Beach TG, Bilker WB, Mintun MA, Pontecorvo MJ,
635 Hefti F, Carpenter AP, Flitter ML, Krautkramer MJ, Kung HF, Coleman RE, Doraiswamy
636 PM, Fleisher AS, Sabbagh MN, Sadowsky CH, Reiman EM, Zehntner SP, Skovronsky
637 DM, Group for the A-AS (2011) Use of Florbetapir-PET for Imaging β-Amyloid
638 Pathology. JAMA 305:275–283. doi: 10.1001/JAMA.2010.2008
639 13. Corrada MM, Sonnen JA, Kim RC, Kawas CH (2016) Microinfarcts are common and
640 strongly related to dementia in the oldest-old: The 90+ study. Alzheimer's Dement

12:900–908. doi: 10.1016/j.jalz.2016.04.006

14. Curtis C, Gamez JE, Singh U, Sadowsky CH, Villena T, Sabbagh MN, Beach TG, Duara R, Fleisher AS, Frey KA, Walker Z, Hunjan A, Holmes C, Escovar YM, Vera CX, Agronin ME, Ross J, Bozoki A, Akinola M, Shi J, Vandenberghe R, Ikonomovic MD, Sherwin PF, Grachev ID, Farrar G, Smith APL, Buckley CJ, McLain R, Salloway S (2015) Phase 3 trial of flutemetamol labeled with radioactive fluorine 18 imaging and neuritic plaque density. JAMA Neurol 72:287–294. doi: 10.1001/jamaneurol.2014.4144

15. Davies CA, Mann DMA (1993) Is the "preamyloid" of diffuse plaques in Alzheimer's disease really nonfibrillar? Am J Pathol 143:1594–1605

16. Dickson TC, Vickers JC (2001) The morphological phenotype of β-amyloid plaques and associated neuritic changes in Alzheimer's disease. Neuroscience 105:99–107. doi: 10.1016/S0306-4522(01)00169-5

17. Ding T, Wu T, Mazidi H, Zhang O, Lew MD (2020) Single-molecule orientation localization microscopy for resolving structural heterogeneities between amyloid fibrils. Optica 7:602. doi: 10.1364/optica.388157

18. Driscoll I, Troncoso JC, Rudow G, Sojkova J, Pletnikova O, Zhou Y, Kraut MA, Ferrucci L, Mathis CA, Klunk WE, O'Brien RJ, Davatzikos C, Wong DF, Resnick SM (2012) Correspondence between in vivo 11C-PiB-PET amyloid imaging and postmortem, region-matched assessment of plaques. Acta Neuropathol 124:823–831. doi: 10.1007/s00401-012-1025-1

19. Efron B (2007) Size, power and false discovery rates. Ann Stat 35:1351–1377. doi: 10.1214/009053606000001460

20. Van Essen DC, Jbabdi S, Sotiropoulos SN, Chen C, Dikranian K, Coalson T, Harwell J,

664 Behrens TEJ, Glasser MF (2013) Mapping Connections in Humans and Non-Human
665 Primates. Aspirations and Challenges for Diffusion Imaging. In: Diffusion MRI: From
666 Quantitative Measurement to In vivo Neuroanatomy: Second Edition. Elsevier Inc., pp
667 337–358
668 21. Di Fede G, Catania M, Maderna E, Ghidoni R, Benussi L, Tonoli E, Giaccone G, Moda F,
669 Paterlini A, Campagnani I, Sorrentino S, Colombo L, Kubis A, Bistaffa E, Ghetti B,
670 Tagliavini F (2018) Molecular subtypes of Alzheimer's disease. Sci Rep 8. doi:
671 10.1038/s41598-018-21641-1
672 22. Fischl B, Salat DH, Busa E, Albert M, Dieterich M, Haselgrove C, Van Der Kouwe A,
673 Killiany R, Kennedy D, Klaveness S, Montillo A, Makris N, Rosen B, Dale AM (2002)
674 Whole brain segmentation: Automated labeling of neuroanatomical structures in the
675 human brain. Neuron 33:341–355. doi: 10.1016/S0896-6273(02)00569-X
676 23. Frucht SJ, Koo EH (1993) β-amyloid protein is higher in alzheimer's disease brains:
677 Description of aquantitative biochemical assay. J Neuropathol Exp Neurol 52:640–647.
678 doi: 10.1097/00005072-199311000-00011
679 24. Gordon BA, Blazey TM, Su Y, Hari-Raj A, Dincer A, Flores S, Christensen J, McDade E,
680 Wang G, Xiong C, Cairns NJ, Hassenstab J, Marcus DS, Fagan AM, Jack CR, Hornbeck
681 RC, Paumier KL, Ances BM, Berman SB, Brickman AM, Cash DM, Chhatwal JP,
682 Correia S, Förster S, Fox NC, Graff-Radford NR, la Fougère C, Levin J, Masters CL,
683 Rossor MN, Salloway S, Saykin AJ, Schofield PR, Thompson PM, Weiner MM,
684 Holtzman DM, Raichle ME, Morris JC, Bateman RJ, Benzinger TLS (2018) Spatial
685 patterns of neuroimaging biomarker change in individuals from families with autosomal
686 dominant Alzheimer's disease: a longitudinal study. Lancet Neurol 17:241–250. doi:

687 10.1016/S1474-4422(18)30028-0
688 25. Gravina SA, Ho L, Eckman CB, Long KE, Otvos L, Younkin LH, Suzuki N, Younkin SG
689 (1995) Amyloid β protein (Aβ) in Alzheimer's disease brain. Biochemical and
690 immunocytochemical analysis with antibodies specific for forms ending at Aβ40 or
691 Aβ42(43). J Biol Chem 270:7013–7016. doi: 10.1074/jbc.270.13.7013
692 26. Grothe MJ, Barthel H, Sepulcre J, Dyrba M, Sabri O, Teipel SJ (2017) In vivo staging of
693 regional amyloid deposition. Neurology 89:2031–2038. doi:
694 10.1212/WNL.0000000000004643
695 27. Hanseeuw BJ, Betensky RA, Mormino EC, Schultz AP, Sepulcre J, Becker JA, Jacobs
696 HIL, Buckley RF, LaPoint MR, Vannini P, Donovan NJ, Chhatwal JP, Marshall GA, Papp
697 K V., Amariglio RE, Rentz DM, Sperling RA, Johnson KA (2018) PET staging of
698 amyloidosis using striatum. Alzheimer's Dement 14:1281–1292. doi:
699 10.1016/j.jalz.2018.04.011
700 28. Hyman BT, Phelps CH, Beach TG, Bigio EH, Cairns NJ, Carrillo MC, Dickson DW,
701 Duyckaerts C, Frosch MP, Masliah E, Mirra SS, Nelson PT, Schneider JA, Thal DR,
702 Thies B, Trojanowski JQ, Vinters H V., Montine TJ (2012) National Institute on Aging-
703 Alzheimer's Association guidelines for the neuropathologic assessment of Alzheimer's
704 disease. Alzheimer's Dement 8:1–13. doi: 10.1016/j.jalz.2011.10.007
705 29. Hyman BT, Phelps CH, Beach TG, Bigio EH, Cairns NJ, Carrillo MC, Dickson DW,
706 Duyckaerts C, Frosch MP, Masliah E, Mirra SS, Nelson PT, Schneider JA, Thal DR,
707 Thies B, Trojanowski JQ, Vinters H V., Montine TJ (2012) National Institute on Aging-
708 Alzheimer's Association guidelines for the neuropathologic assessment of Alzheimer's
709 disease. Alzheimer's Dement 8:1–13. doi: 10.1016/j.jalz.2011.10.007

30. Ikonomovic MD, Buckley CJ, Heurling K, Sherwin P, Jones PA, Zanette M, Mathis CA, Klunk WE, Chakrabarty A, Ironside J, Ismail A, Smith C, Thal DR, Beach TG, Farrar G, Smith APL (2016) Post-mortem histopathology underlying β-amyloid PET imaging following flutemetamol F 18 injection. Acta Neuropathol Commun 4:130. doi: 10.1186/s40478-016-0399-z

31. Ikonomovic MD, Klunk WE, Abrahamson EE, Mathis CA, Price JC, Tsopelas ND, Lopresti BJ, Ziolko S, Bi W, Paljug WR, Debnath ML, Hope CE, Isanski BA, Hamilton RL, DeKosky ST (2008) Post-mortem correlates of in vivo PiB-PET amyloid imaging in a typical case of Alzheimer's disease. Brain 131:1630–1645. doi: 10.1093/brain/awn016

32. Jack CR, Knopman DS, Jagust WJ, Petersen RC, Weiner MW, Aisen PS, Shaw LM, Vemuri P, Wiste HJ, Weigand SD, Lesnick TG, Pankratz VS, Donohue MC, Trojanowski JQ (2013) Tracking pathophysiological processes in Alzheimer's disease: An updated hypothetical model of dynamic biomarkers. Lancet Neurol. 12:207–216

33. Jack CR, Knopman DS, Jagust WJ, Shaw LM, Aisen PS, Weiner MW, Petersen RC, Trojanowski JQ (2010) Hypothetical model of dynamic biomarkers of the Alzheimer's pathological cascade. Lancet Neurol. 9:119–128

34. Johnson KA, Gregas M, Becker JA, Kinnecom C, Salat DH, Moran EK, Smith EE, Rosand J, Rentz DM, Klunk WE, Mathis CA, Price JC, DeKosky ST, Fischman AJ, Greenberg SM (2007) Imaging of amyloid burden and distribution in cerebral amyloid angiopathy. Ann Neurol 62:229–234. doi: 10.1002/ana.21164

35. La Joie R, Ayakta N, Seeley WW, Borys E, Boxer AL, DeCarli C, Doré V, Grinberg LT, Huang E, Hwang JH, Ikonomovic MD, Jack C, Jagust WJ, Jin LW, Klunk WE, Kofler J, Lesman-Segev OH, Lockhart SN, Lowe VJ, Masters CL, Mathis CA, McLean CL, Miller

733 BL, Mungas D, O'Neil JP, Olichney JM, Parisi JE, Petersen RC, Rosen HJ, Rowe CC,
734 Spina S, Vemuri P, Villemagne VL, Murray ME, Rabinovici GD (2019) Multisite study of
735 the relationships between antemortem [11 C]PIB-PET Centiloid values and postmortem
736 measures of Alzheimer's disease neuropathology. Alzheimer's Dement 15:205–216. doi:
737 10.1016/j.jalz.2018.09.001
738 36. Klunk WE, Engler H, Nordberg A, Wang Y, Blomqvist G, Holt DP, Bergström M,
739 Savitcheva I, Huang GF, Estrada S, Ausén B, Debnath ML, Barletta J, Price JC, Sandell J,
740 Lopresti BJ, Wall A, Koivisto P, Antoni G, Mathis CA, Långström B (2004) Imaging
741 Brain Amyloid in Alzheimer's Disease with Pittsburgh Compound-B. Ann Neurol
742 55:306–319. doi: 10.1002/ana.20009
743 37. Klunk WE, Koeppe RA, Price JC, Benzinger TL, Devous MD, Jagust WJ, Johnson KA,
744 Mathis CA, Minhas D, Pontecorvo MJ, Rowe CC, Skovronsky DM, Mintun MA (2015)
745 The Centiloid project: Standardizing quantitative amyloid plaque estimation by PET.
746 Alzheimer's Dement 11:1-15.e4. doi: 10.1016/j.jalz.2014.07.003
747 38. Klunk WE, Lopresti BJ, Ikonomovic MD, Lefterov IM, Koldamova RP, Abrahamson EE,
748 Debnath ML, Holt DP, Huang GF, Shao L, DeKosky ST, Price JC, Mathis CA (2005)
749 Binding of the positron emission tomography tracer Pittsburgh Compound-B reflects the
750 amount of amyloid-β in Alzheimer's Disease brain but not in transgenic mouse brain. J
751 Neurosci 25:10598–10606. doi: 10.1523/JNEUROSCI.2990-05.2005
752 39. Klunk WE, Price JC, Mathis CA, Tsopelas ND, Lopresti BJ, Ziolko SK, Bi W, Hoge JA,
753 Cohen AD, Ikonomovic MD, Saxton JA, Snitz BE, Pollen DA, Moonis M, Lippa CF,
754 Swearer JM, Johnson KA, Rentz DM, Fischman AJ, Aizenstein HJ, DeKosky ST (2007)
755 Amyloid deposition begins in the striatum of presenilin-1 mutation carriers from two

unrelated pedigrees. J Neurosci 27:6174–6184. doi: 10.1523/JNEUROSCI.0730-07.2007

40. Knowles RB, Wyart C, Buldyrev S V., Cruz L, Urbanc B, Hasselmo ME, Stanley HE, Hyman BT (1999) Plaque-induced neurite abnormalities: Implications for disruption of neural networks in Alzheimer's disease. Proc Natl Acad Sci U S A 96:5274–5279. doi: 10.1073/pnas.96.9.5274

41. Koivunen J, Verkkoniemi A, Aalto S, Paetau A, Ahonen JP, Viitanen M, Någren K, Rokka J, Haaparanta M, Kalimo H, Rinne JO (2008) PET amyloid ligand [11C]PIB uptake shows predominantly striatal increase in variant Alzheimer's disease. Brain 131:1845–1853. doi: 10.1093/brain/awn107

42. Larner AJ, Doran M (2006) Clinical phenotypic heterogeneity of Alzheimer's disease associated with mutations of the presenilin-1 gene. J. Neurol. 253:139–158

43. Lockhart A, Lamb JR, Osredkar T, Sue LI, Joyce JN, Ye L, Libri V, Leppert D, Beach TG (2007) PIB is a non-specific imaging marker of amyloid-beta (Aβ) peptide-related cerebral amyloidosis. Brain 130:2607–2615. doi: 10.1093/brain/awm191

44. Lowe VJ, Lundt ES, Senjem ML, Schwarz CG, Min HK, Przybelski SA, Kantarci K, Knopman D, Petersen RC, Jack CR (2018) White matter reference region in PET studies of 11C-Pittsburgh compound B uptake: Effects of age and amyloid-β deposition. J Nucl Med 59:1583–1589. doi: 10.2967/jnumed.117.204271

45. Ly J V., Donnan GA, Villemagne VL, Zavala JA, Ma H, O'Keefe G, Gong SJ, Gunawan RM, Saunder T, Ackerman U, Tochon-Danguy H, Churilov L, Phan TG, Rowe CC (2010) 11C-PIB binding is increased in patients with cerebral amyloid angiopathy-related hemorrhage. Neurology 74:487–493. doi: 10.1212/WNL.0b013e3181cef7e3

46. Maarouf CL, Daugs ID, Spina S, Vidal R, Kokjohn TA, Patton RL, Kalback WM, Luehrs

779 DC, Walker DG, Castaño EM, Beach TG, Ghetti B, Roher AE (2008) Histopathological
780 and molecular heterogeneity among individuals with dementia associated with Presenilin
781 mutations. Mol Neurodegener 3:20. doi: 10.1186/1750-1326-3-20
782 47. Mirra SS, Heyman A, McKeel D, Sumi SM, Crain BJ, Brownlee LM, Vogel FS, Hughes
783 JP, van Belle G, Berg L, Ball MJ, Bierer LM, Claasen D, Hansen LR, Hart M, Hedreen J,
784 Baltimore B, Hen Derson V, Hyman BT, Joachim C, Mark-Esbery W, Mar Tinez AJ,
785 McKee A, Miller C, Moossy J, Nochlin D, Perl D, Petito C, Rao GR, Schelper RL, Slager
786 U, Terry RD (1991) The consortium to establish a registry for Alzheimer's disease
787 (CERAD). Part II. Standardization of the neuropathologic assessment of Alzheimer's
788 disease. Neurology 41:479–486. doi: 10.1212/wnl.41.4.479
789 48. Montine TJ, Phelps CH, Beach TG, Bigio EH, Cairns NJ, Dickson DW, Duyckaerts C,
790 Frosch MP, Masliah E, Mirra SS, Nelson PT, Schneider JA, Thal DR, Trojanowski JQ,
791 Vinters H V., Hyman BT (2012) National institute on aging-Alzheimer's association
792 guidelines for the neuropathologic assessment of Alzheimer's disease: A practical
793 approach. Acta Neuropathol 123:1–11. doi: 10.1007/s00401-011-0910-3
794 49. Morris JC, Aisen PS, Bateman RJ, Benzinger TL, Cairns NJ, Fagan AM, Ghetti B, Goate
795 AM, Holtzman DM, Klunk WE, McDade E, Marcus DS, Martins RN, Masters CL,
796 Mayeux R, Oliver A, Quaid K, M Ringman J, Rossor MN, Salloway S, Schofield PR,
797 Selsor NJ, Sperling RA, Weiner MW, Xiong C, Moulder KL, Buckles VD (2012)
798 Developing an international network for Alzheimer's research: the Dominantly Inherited
799 Alzheimer Network. Clin Investig (Lond) 2:975–984. doi: 10.4155/cli.12.93
800 50. Murray ME, Lowe VJ, Graff-Radford NR, Liesinger AM, Cannon A, Przybelski SA,
801 Rawal B, Parisi JE, Petersen RC, Kantarci K, Ross OA, Duara R, Knopman DS, Jack CR,

802 Dickson DW (2015) Clinicopathologic and 11C-Pittsburgh compound B implications of
803 Thal amyloid phase across the Alzheimer's disease spectrum. Brain 138:1370–1381. doi:
804 10.1093/brain/awv050
805 51. Nelson PT, Alafuzoff I, Bigio EH, Bouras C, Braak H, Cairns NJ, Castellani RJ, Crain BJ,
806 Davies P, Tredici K Del, Duyckaerts C, Frosch MP, Haroutunian V, Hof PR, Hulette CM,
807 Hyman BT, Iwatsubo T, Jellinger KA, Jicha GA, Kövari E, Kukull WA, Leverenz JB,
808 Love S, MacKenzie IR, Mann DM, Masliah E, McKee AC, Montine TJ, Morris JC,
809 Schneider JA, Sonnen JA, Thal DR, Trojanowski JQ, Troncoso JC, Wisniewski T, Woltjer
810 RL, Beach TG (2012) Correlation of alzheimer disease neuropathologic changes with
811 cognitive status: A review of the literature. J. Neuropathol. Exp. Neurol. 71:362–381
812 52. Nelson PT, Dickson DW, Trojanowski JQ, Jack CR, Boyle PA, Arfanakis K, Rademakers
813 R, Alafuzoff I, Attems J, Brayne C, Coyle-Gilchrist ITS, Chui HC, Fardo DW, Flanagan
814 ME, Halliday G, Hokkanen SRK, Hunter S, Jicha GA, Katsumata Y, Kawas CH, Keene
815 CD, Kovacs GG, Kukull WA, Levey AI, Makkinejad N, Montine TJ, Murayama S,
816 Murray ME, Nag S, Rissman RA, Seeley WW, Sperling RA, White CL, Yu L, Schneider
817 JA (2019) Limbic-predominant age-related TDP-43 encephalopathy (LATE): Consensus
818 working group report. Brain 142:1503–1527
819 53. Olichney JM, Hansen LA, Hofstetter CR, Lee JH, Katzman R, Thal LJ (2000) Association
820 between severe cerebral amyloid angiopathy and cerebrovascular lesions in Alzheimer
821 disease is not a spurious one attributable to apolipoprotein E4. Arch Neurol 57:869–874.
822 doi: 10.1001/archneur.57.6.869
823 54. Portelius E, Andreasson U, Ringman JM, Buerger K, Daborg J, Buchhave P, Hansson O,
824 Harmsen A, Gustavsson MK, Hanse E, Galasko D, Hampel H, Blennow K, Zetterberg H

(2010) Distinct cerebrospinal fluid amyloid peptide signatures in sporadic and PSEN1 A431E-associated familial Alzheimer's disease. Mol Neurodegener 5:2. doi: 10.1186/1750-1326-5-2

55. Price JL, McKeel DW, Buckles VD, Roe CM, Xiong C, Grundman M, Hansen LA, Petersen RC, Parisi JE, Dickson DW, Smith CD, Davis DG, Schmitt FA, Markesbery WR, Kaye J, Kurlan R, Hulette C, Kurland BF, Higdon R, Kukull W, Morris JC (2009) Neuropathology of nondemented aging: Presumptive evidence for preclinical Alzheimer disease. Neurobiol Aging 30:1026–1036. doi: 10.1016/j.neurobiolaging.2009.04.002

56. Remes AM, Laru L, Tuominen H, Aalto S, Kemppainen N, Mononen H, Någren K, Parkkola R, Rinne JO (2008) Carbon 11-labeled Pittsburgh Compound B positron emission tomographic amyloid imaging in patients with APP locus duplication. Arch Neurol 65:540–544. doi: 10.1001/archneur.65.4.540

57. Ringman JM, Monsell S, Ng DW, Zhou Y, Nguyen A, Coppola G, Berlo V Van, Mendez MF, Tung S, Weintraub S, Mesulam M-M, Bigio EH, Gitelman DR, Fisher-Hubbard AO, Albin RL, Vinters H V. (2016) Neuropathology of Autosomal Dominant Alzheimer Disease in the National Alzheimer Coordinating Center Database. J Neuropathol Exp Neurol 75:284. doi: 10.1093/JNEN/NLV028

58. Roberts BR, Lind M, Wagen AZ, Rembach A, Frugier T, Li QX, Ryan TM, McLean CA, Doecke JD, Rowe CC, Villemagne VL, Masters CL (2017) Biochemically-defined pools of amyloid-β in sporadic Alzheimer's disease: Correlation with amyloid PET. Brain 140:1486–1498. doi: 10.1093/brain/awx057

59. Ryman DC, Acosta-Baena N, Aisen PS, Bird T, Danek A, Fox NC, Goate A, Frommelt P, Ghetti B, Langbaum JBS, Lopera F, Martins R, Masters CL, Mayeux RP, McDade E,

Moreno S, Reiman EM, Ringman JM, Salloway S, Schofield PR, Sperling R, Tariot PN, Xiong C, Morris JC, Bateman RJ (2014) Symptom onset in autosomal dominant Alzheimer disease: A systematic review and meta-analysis. Neurology 83:253–260. doi: 10.1212/WNL.0000000000000596

60. Sabri O, Sabbagh MN, Seibyl J, Barthel H, Akatsu H, Ouchi Y, Senda K, Murayama S, Ishii K, Takao M, Beach TG, Rowe CC, Leverenz JB, Ghetti B, Ironside JW, Catafau AM, Stephens AW, Mueller A, Koglin N, Hoffmann A, Roth K, Reininger C, Schulz-Schaeffer WJ (2015) Florbetaben PET imaging to detect amyloid beta plaques in Alzheimer's disease: Phase 3 study. Alzheimer's Dement 11:964–974. doi: 10.1016/j.jalz.2015.02.004

61. Schöll M, Wall A, Thordardottir S, Ferreira D, Bogdanovic N, Långström B, Almkvist O, Graff C, Nordberg A (2012) Low PiB PET retention in presence of pathologic CSF biomarkers in Arctic APP mutation carriers. Neurology 79:229–236. doi: 10.1212/WNL.0b013e31825fdf18

62. Sepulveda-Falla D, Chavez-Gutierrez L, Portelius E, Vélez JI, Barrera-Ocampo A, Dinkel F, Hagel C, Puig B, Mastronardi C, Lopera F, Blennow K, Arcos-Burgos M, de Strooper B, Glatzel M (2018) A multifactorial model of pathology for age of onset variability in Familial Alzheimer's disease. Sci Transl Med revised ve. doi: 10.1007/s00401-020-02249-0

63. Su Y, Blazey TM, Snyder AZ, Raichle ME, Marcus DS, Ances BM, Bateman RJ, Cairns NJ, Aldea P, Cash L, Christensen JJ, Friedrichsen K, Hornbeck RC, Farrar AM, Owen CJ, Mayeux R, Brickman AM, Klunk W, Price JC, Thompson PM, Ghetti B, Saykin AJ, Sperling RA, Johnson KA, Schofield PR, Buckles V, Morris JC, Benzinger TLS (2015)

Partial volume correction in quantitative amyloid imaging. Neuroimage 107:55–64. doi: 10.1016/j.neuroimage.2014.11.058

64. Su Y, D'Angelo GM, Vlassenko AG, Zhou G, Snyder AZ, Marcus DS, Blazey TM, Christensen JJ, Vora S, Morris JC, Mintun MA, Benzinger TLS (2013) Quantitative Analysis of PiB-PET with FreeSurfer ROIs. PLoS One 8:e73377. doi: 10.1371/journal.pone.0073377

65. Su Y, Flores S, Hornbeck RC, Speidel B, Vlassenko AG, Gordon BA, Koeppe RA, Klunk WE, Xiong C, Morris JC, Benzinger TLS (2018) Utilizing the Centiloid scale in cross-sectional and longitudinal PiB PET studies. NeuroImage Clin 19:406–416. doi: 10.1016/j.nicl.2018.04.022

66. Tang M, Ryman DC, McDade E, Jasielec MS, Buckles VD, Cairns NJ, Fagan AM, Goate A, Marcus DS, Xiong C, Allegri RF, Chhatwal JP, Danek A, Farlow MR, Fox NC, Ghetti B, Graff-Radford NR, Laske C, Martins RN, Masters CL, Mayeux RP, Ringman JM, Rossor MN, Salloway SP, Schofield PR, Morris JC, Bateman RJ (2016) Neurological manifestations of autosomal dominant familial Alzheimer's disease: a comparison of the published literature with the Dominantly Inherited Alzheimer Network observational study (DIAN-OBS). Lancet Neurol 15:1317–1325. doi: 10.1016/S1474-4422(16)30229-0

67. Thal DR, Beach TG, Zanette M, Lilja J, Heurling K, Chakrabarty A, Ismail A, Farrar G, Buckley C, Smith APL (2018) Estimation of amyloid distribution by [18F]flutemetamol PET predicts the neuropathological phase of amyloid β-protein deposition. Acta Neuropathol 136:557–567. doi: 10.1007/s00401-018-1897-9

68. Thal DR, Ronisz A, Tousseyn T, Rijal Upadhaya A, Balakrishnan K, Vandenberghe R, Vandenbulcke M, Von Arnim CAF, Otto M, Beach TG, Lilja J, Heurling K, Chakrabarty

A, Ismail A, Buckley C, Smith APL, Kumar S, Farrar G, Walter J (2019) Different aspects of Alzheimer's disease-related amyloid β-peptide pathology and their relationship to amyloid positron emission tomography imaging and dementia. Acta Neuropathol Commun 7:178. doi: 10.1186/s40478-019-0837-9

69. Thal DR, Rüb U, Orantes M, Braak H (2002) Phases of Aβ-deposition in the human brain and its relevance for the development of AD. Neurology 58:1791–1800. doi: 10.1212/WNL.58.12.1791

70. Theuns J, Marjaux E, Vandenbulcke M, Van Laere K, Kumar-Singh S, Bormans G, Brouwers N, Van Den Broeck M, Vennekens K, Corsmit E, Cruts M, De Strooper B, Van Broeckhoven C, Vandenberghe R (2006) Alzheimer dementia caused by a novel mutation located in the APP C-terminal intracytosolic fragment. Hum Mutat 27:888–896. doi: 10.1002/humu.20402

71. Thiyagarajan P, Burkoth TS, Urban V, Seifert S, Benzinger TLS, Morgan DM, Gordon D, Meredith SC, Lynn DG (2000) pH dependent self assembly of β-amyloid(10-35) and β-amyloid(10-35)-PEG3000. In: Journal of Applied Crystallography. pp 535–539

72. Tomiyama T, Nagata T, Shimada H, Teraoka R, Fukushima A, Kanemitsu H, Takuma H, Kuwano R, Imagawa M, Ataka S, Wada Y, Yoshioka E, Nishizaki T, Watanabe Y, Mori H (2008) A new amyloid β variant favoring oligomerization in Alzheimer's-type dementia. Ann Neurol 63:377–387. doi: 10.1002/ana.21321

73. Verwey NA, Hoozemans JJM, Korth C, Van Royen MR, Prikulis I, Wouters D, Twaalfhoven HAM, Van Haastert ES, Schenk D, Scheltens P, Rozemuller AJM, Blankenstein MA, Veerhuis R (2013) Immunohistochemical characterization of novel monoclonal antibodies against the N-terminus of amyloid β-peptide. Amyloid 20:179–

187. doi: 10.3109/13506129.2013.797389

74. Villemagne VL, Burnham S, Bourgeat P, Brown B, Ellis KA, Salvado O, Szoeke C, Macaulay SL, Martins R, Maruff P, Ames D, Rowe CC, Masters CL (2013) Amyloid β deposition, neurodegeneration, and cognitive decline in sporadic Alzheimer's disease: A prospective cohort study. Lancet Neurol 12:357–367. doi: 10.1016/S1474-4422(13)70044-9

75. Vonsattel JPG, Myers RH, Tessa Hedley-Whyte E, Ropper AH, Bird ED, Richardson EP (1991) Cerebral amyloid angiopathy without and with cerebral hemorrhages: A comparative histological study. Ann Neurol 30:637–649. doi: 10.1002/ana.410300503

76. Wong DF, Rosenberg PB, Zhou Y, Kumar A, Raymont V, Ravert HT, Dannals RF, Nandi A, Bra̧šić JR, Ye W, Hilton J, Lyketsos C, Kung HF, Joshi AD, Skovronsky DM, Pontecorvo MJ (2010) In vivo imaging of amyloid deposition in Alzheimer disease using the radioligand 18F-AV-45 (flobetapir F 18). J Nucl Med 51:913–920. doi: 10.2967/jnumed.109.069088

Tables and figure legends

Table 1 Cohort demographics

ADAD	Family mutation	*APOE*	Sex	MMSE	CDR	Clinical cause of death	CDR at death	Age at death	Imaging-autopsy interval (years)	Thal phase	Braak stage	CERAD score	CAA	Final Dx 1	Final Dx 2-4
1	*PSEN1*	44	M	21	1	Aspiration, pneumonia, AD	3	40-50	0.68	5	6	3	1	ADNC	Glioblastoma
2	*PSEN1*	23	F	16	1	Probable pneumonia	3	30-40	1.1	5	6	3	1	ADNC	
3	*PSEN1*	33	M	9	3	Inanition	3	40-50	1	5	6	3	2	ADNC	DLB (neocortical), SVD: CAA (moderate-severe), Art. (mild)
4	*PSEN1*	34	F	21	1	AD	3	40-50	3.3	5	6	3	3	ADNC	DLB
5	*PSEN1*	23	F	12	2	Probable pneumonia	3	40-50	2.3	5	6	3	2	ADNC	
6	*PSEN1*	33	M	10	1	AD, inanition		40-50	1.8	5	6	3	1	ADNC	DLB
7	*PSEN1*	33	M	13	2	AD, inanition	3	50-60	1.3	5	6	3	1	ADNC	ALB
8	*PSEN1*	23	F	8	2	Respiratory failure, cardiac arrest, AD	3	40-50	1.5	5	6	3	1	ADNC	MH (BG)
9	*PSEN1*	34	F	21	0.5	AD	3	30-40	2.5	5	6	3	3	ADNC	
10	*PSEN1*	33	M	0	3	Heart attack, Inanition	3	60-70	4	5	6	3	1	ADNC	ALB
11	*PSEN1*	34	F	8	3	AD, inanition	3	40-50	2.3	5	6	3	3	ADNC	ALB
12	*PSEN1*	33	M	15	1	Aspiration, inanition	3	50-60	2	5	6	3	3	ADNC	CAA
13	*PSEN1*	33	M	19	1	Brain hemorrhage, inanition	3	50-60	3.4	5	6	3	2	ADNC	ALB
14	*APP*	44	M	21	2	Pneumonia, inanition	3	60-70	5.6	5	6	3	3	ADNC	ALB
15	*PSEN1*	33	M	27	0.5	AD	3	30-40	3.3	5	6	3	3	ADNC	
Mean (SD)				15 (7)	1.6 (0.9)		3 (0)	47 (9)	2.4 (1.3)	5 (0)	6 (0)	3 (0)	2 (0.9)		
LOAD	**Family mutation**	***APOE***	**Sex**	**MMSE**	**CDR**	**Clinical cause of death**	**CDR at death**	**Age at death**	**Imaging-autopsy interval**	**Thal phase**	**Braak stage**	**CERAD score**	**CAA**	**Final Dx 1**	**Final Dx 2-4**
1		34	M	30	0.5	UTI, diabetes mellitus, AD contributing	2	80-90	3.7	5	5	3	1	ADNC	SVD: Art. (moderate), LVD: Art. (moderate)
2		33	M	21	1	Lymphoma	2	60-70	3.9	5	6	3	1	ADNC	
3		34	F	20	1	AD	3	80-90	3.8	5	5	3	1	ADNC	
4		34	F	26	0.5	Inanition	3	70-80	3.9	5	5	3	3	ADNC	
5		34	M	12	2	AD	3	70-80	4.7	5	5	3	1	ADNC	

6	34	F	28	0	AD	3	80-90	4.8	5	4	3	1	ADNC	
7	34	M	25	0.5	DLB, UTI, dehydration	3	70-80	3.7	5	5	3	1	ADNC	
8	33	M	22	1		1	80-90	0.3	5	5	3	1	ADNC	
9	34	M	26	0.5	Inanition	3	80-90	3.4	4	5	3	1	ADNC	
10	34	F	25	0.5	Inanition	3	90-100	8.4	4	6	3	2	ADNC	Infarcts (BG, Th)
11	34	M	26	0.5	Inanition	3	90-100	9.6	5	5	3	3	ADNC	ALB, TDP-43 (MTL)
12	34	M	23	0.5	Inanition	3	70-80	4.2	5	5	3	1	ADNC	
13	33	F	25	0.5		2	90-100	6.1	5	5	3	2	ADNC	Infarcts (PL, FL), microinfarct (FL)
14	33	M	23	0.5	AD	3	70-80	4.9	5	6	3	1	ADNC	DLB (olfactory), SVD: Art. (moderate), SVD: CAA (mild)
Mean (SD)			24 (4)	0.7 (0.5)		2.6 (0.6)	83 (9)	4.7 (2.2)		5.1 (0.5)	3 (0)	1.4 (0.8)		

Age at death is reported as an age range to protect the identities of the study participants. Exact ADAD mutations of the *PSEN1* gene are presented in Online Resource 2 in the interests of better understanding the clinicopathologic variability in this population, but are not linked to the individual-level demographics in this table in order to protect the identities of the study participants. Abbreviations: ADNC (Alzheimer disease neuropathologic change), ALB (amygdala Lewy bodies), Art. (arteriolosclerosis), BG (basal ganglia), CAA (cerebral amyloid angiopathy), DLB (dementia with Lewy bodies), Dx (diagnosis), FL (frontal lobe), LVD (large vessel disease), MH (microhemorrhage), MTL (medial temporal lobe), PL (parietal lobe), SAH (subarachnoid hemorrhage), SD (standard deviation), SVD (small vessel disease), Th (thalamus), UTI (urinary tract infection).

Table 2 Regional correlations between [11C]PiB PET SUVRs and plaque area fractions

ADAD	**Diffuse plaque**	**Compact plaque**

Summary regions	*r*	*SE*	*p*	*r*	*SE*	*p*
Anterior cingulate	**0.81**	**0.16**	**0.0018**	0.32	0.26	0.45
Caudate	**0.62**	**0.22**	**0.018**	0.066	0.28	0.87
Frontal lobe	**0.63**	**0.19**	**0.018**	0.31	0.26	0.45
Parietal lobe	**0.70**	**0.20**	**0.012**	0.59	0.22	0.15
Posterior cingulate	**0.63**	**0.22**	**0.018**	0.045	0.28	0.87
Putamen	0.34	0.26	0.21	-0.084	0.28	0.87
Temporal lobe	**0.60**	**0.22**	**0.021**	0.31	0.26	0.45
Other regions						
Amygdala	0.43	0.25	0.11	0.58	0.23	0.053
Entorhinal cortex	0.46	0.25	0.081	0.48	0.24	0.10
Globus pallidus	-0.013	0.28	0.96	0.12	0.28	0.79
Hippocampus	0.29	0.27	0.30	0.56	0.23	0.053
Occipital lobe	**0.80**	**0.17**	**0.00038**	**0.65**	**0.21**	**0.030**
Parahippocampal gyrus	**0.64**	**0.21**	**0.011**	**0.65**	**0.21**	**0.030**
Thalamus	0.48	0.24	0.073	0.059	0.28	0.83
LOAD						
Summary regions						
Anterior cingulate	**0.82**	**0.16**	**0.00098**	**0.68**	**0.21**	**0.018**
Caudate	0.36	0.27	0.25	0.087	0.29	0.77
Frontal lobe	**0.72**	**0.20**	**0.0080**	**0.81**	**0.17**	**0.0028**
Parietal lobe	**0.83**	**0.16**	**0.00098**	**0.62**	**0.23**	**0.030**
Posterior cingulate	0.23	0.28	0.43	0.23	0.28	0.61
Putamen	0.52	0.25	0.077	-0.087	0.29	0.77
Temporal lobe	0.54	0.24	0.077	**0.68**	**0.21**	**0.018**
Other regions						
Amygdala	**0.71**	**0.20**	**0.016**	0.34	0.27	0.32
Entorhinal cortex	0.072	0.29	0.81	-0.44	0.26	0.26
Globus pallidus	0.14	0.29	0.81	0.13	0.29	0.77
Hippocampus	0.081	0.29	0.81	-0.059	0.29	0.84
Occipital lobe	**0.77**	**0.18**	**0.0090**	0.39	0.27	0.29
Parahippocampal gyrus	0.49	0.25	0.14	0.59	0.23	0.18
Thalamus	0.50	0.25	0.14	0.48	0.25	0.26

946 *P*-values are adjusted for FDR control by the Benjamini-Hochberg procedure. Abbreviations: SE

947 (standard error).

948

949 **Table 3** Extended imaging cohort demographics

		ADAD	**LOAD**
Number		317	734
Family mutation	***PSEN1***	131	
	PSEN2	22	
	APP	31	

	Non-carrier	133	
APOE	**22**	3	3
	23	28	80
	24	12	18
	33	191	368
	34	78	209
	44	5	42
Sex	**M**	135	313
	F	182	421
Mean baseline MMSE (SD)		28.8 (8.61)	28.7 (1.86)
Baseline CDR	**0**	251	615
	0.5	43	98
	1	16	21
	2	5	0
	3	2	0
Mean baseline age (SD)		37.7 (10.7)	68.7 (9.49)

Fig. 1 Regional differences between ADAD and LOAD as measured by [11C]PiB PET SUVRs and plaque area fractions

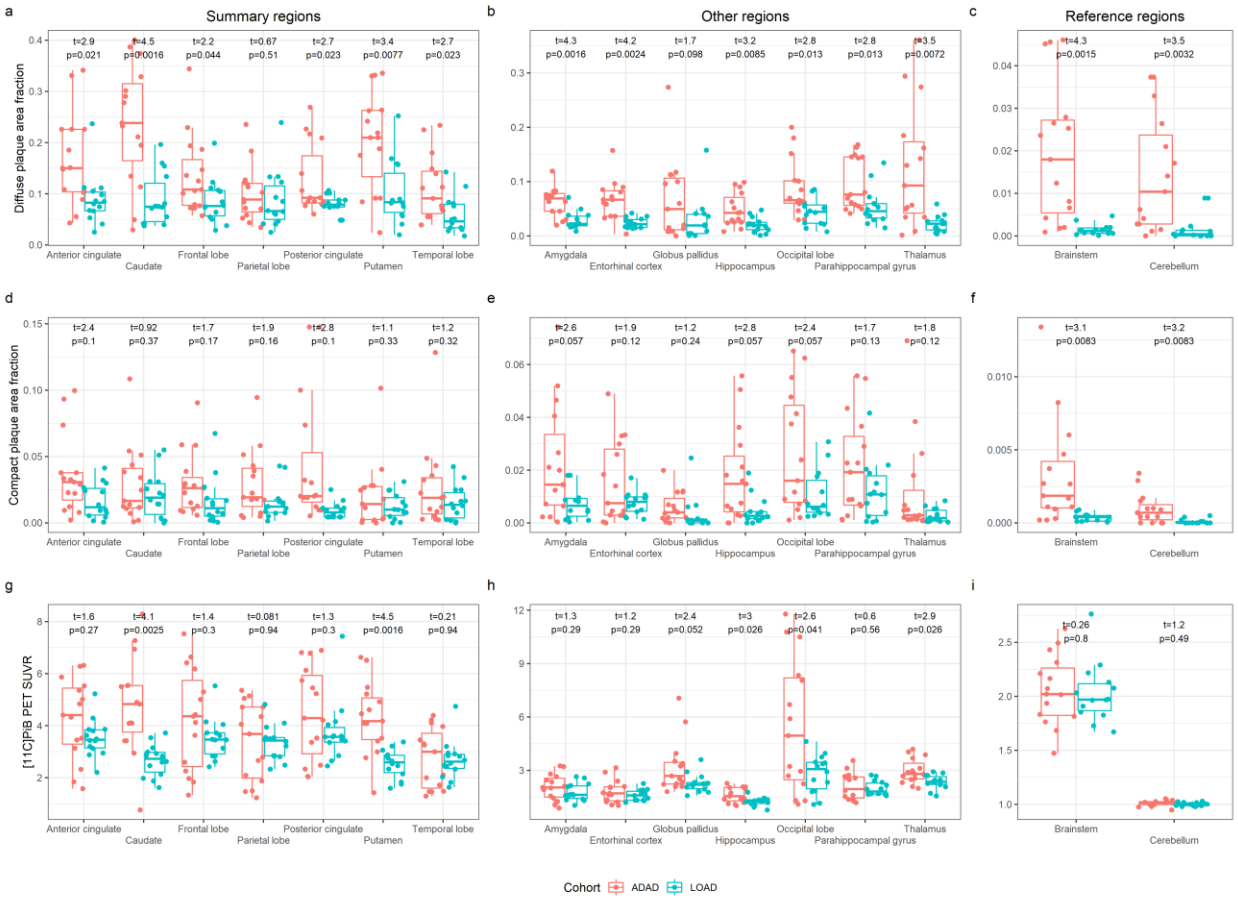

953

954 Regional differences in diffuse (**a**, **b**, **c**) and compact plaque area fractions (**d**, **e**, **f**) and [11C]PiB
955 PET SUVRs (**g**, **h**, **i**) across summary regions, other regions, and reference regions between ADAD
956 and LOAD. Differences are reported as *t*-values from Welch two sample *t*-tests, accompanied by
957 *p*-values adjusted for FDR control by the Benjamini-Hochberg procedure.

958

959 **Fig. 2** Regional differences between ADAD and LOAD as measured by [11C]PiB PET SUVRs
960 while using alternative reference regions

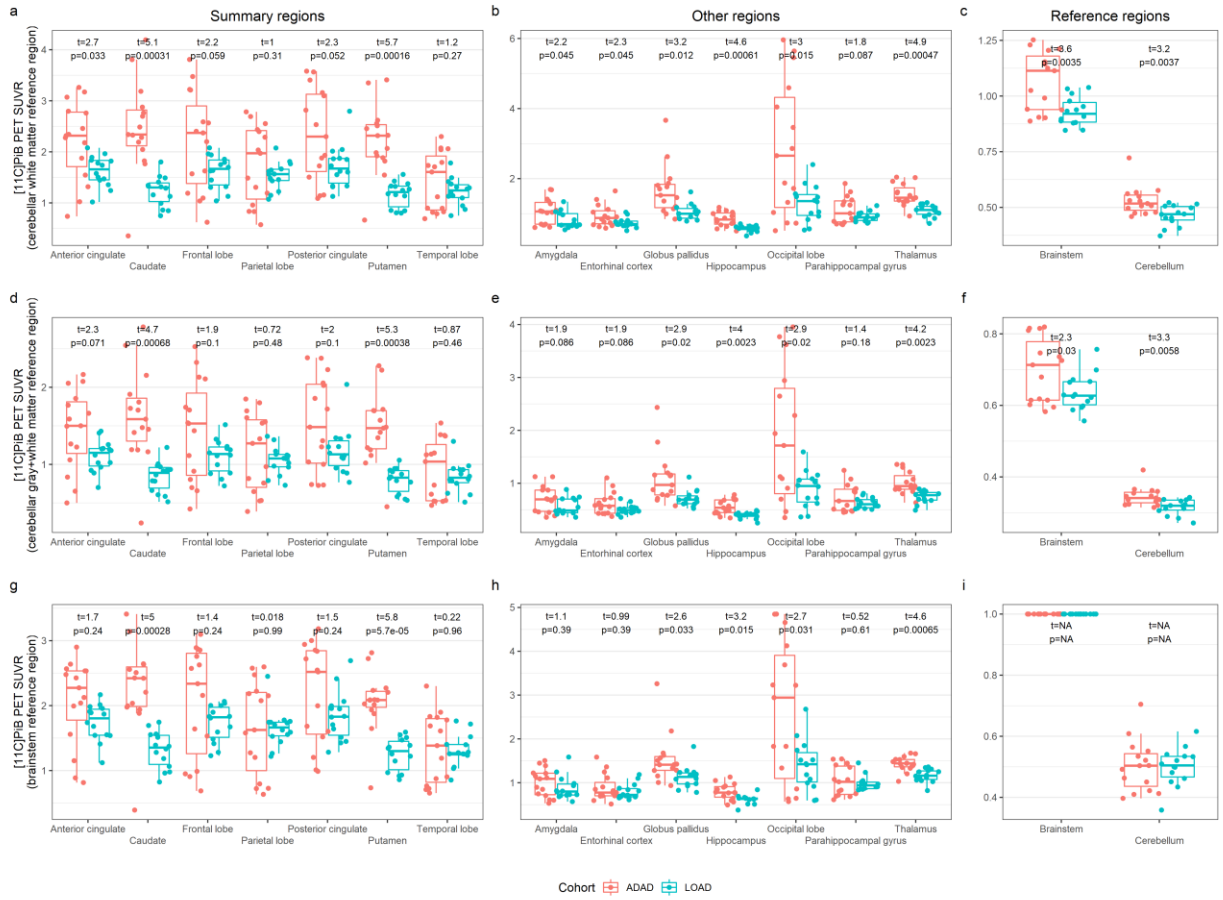

961

962 Regional differences in [11C]PiB PET SUVRs when using cerebellar white (**a**, **b**, **c**), cerebellar
963 gray+white (**d**, **e**, **f**), and brainstem reference regions (**g**, **h**, **i**) between ADAD and LOAD.
964 Differences are reported as *t*-values from Welch two sample *t*-tests, accompanied by *p*-values
965 adjusted for FDR control by the Benjamini-Hochberg procedure.

966

967 **Fig. 3** Regional distributions of PiB PET SUVRs in ADAD and LOAD

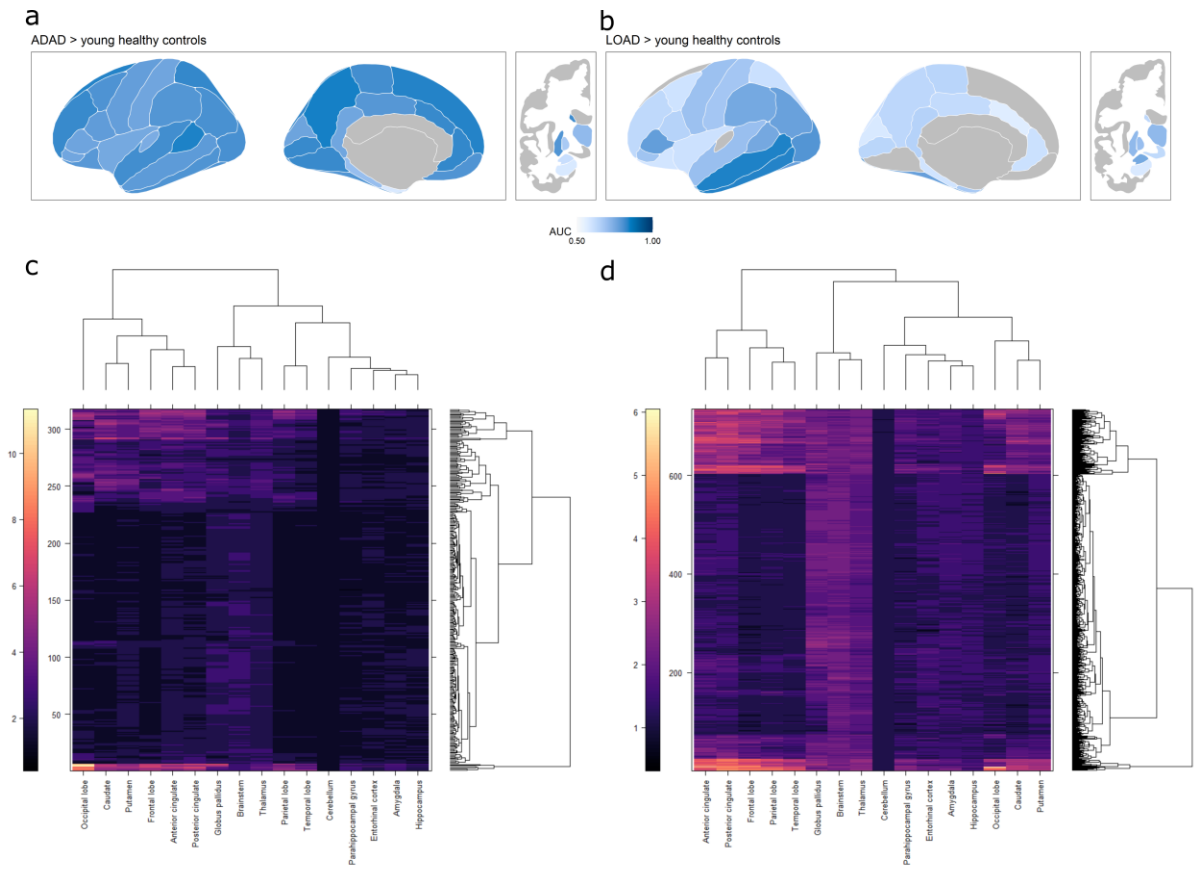

968

969 Regional PiB PET SUVRs in ADAD and LOAD. **a** Regional area under the receiver operating
970 characteristic curves for ADAD versus young healthy controls (AUC, the probability that a
971 randomly selected ADAD participant has a higher regional PiB PET SUVR than a randomly
972 selected young healthy control). **b** Regional AUCs for LOAD versus young healthy controls. **c**
973 Heatmap and dendrograms of ADAD participants after hierarchical agglomerative clustering. **d**
974 Heatmap and dendrograms of LOAD participants after hierarchical agglomerative clustering.

975

976 **Online Resource 1** Matching regions between imaging and neuropathology

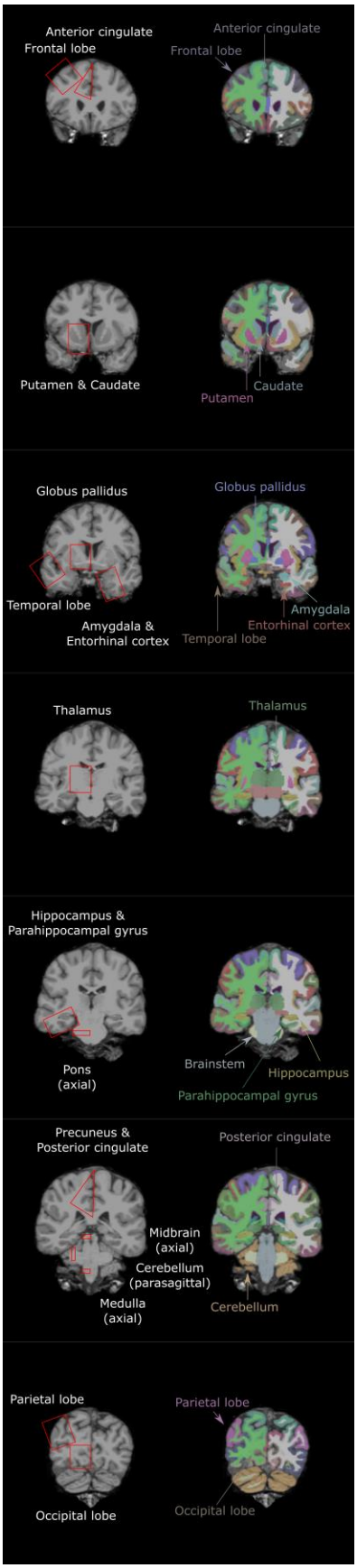
Anterior cingulate
Frontal lobe
Anterior cingulate
Frontal lobe
Putamen & Caudate
Caudate
Putamen
Globus pallidus
Globus pallidus
Temporal lobe
Amygdala
Entorhinal cortex
Amygdala &
Entorhinal cortex
Temporal lobe
Thalamus
Thalamus
Hippocampus &
Parahippocampal gyrus
Pons
(axial)
Brainstem
Hippocampus
Parahippocampal gyrus
Precuneus &
Posterior cingulate
Posterior cingulate
Midbrain
(axial)
Cerebellum
(parasagittal)
Medulla
(axial)
Cerebellum
Parietal lobe
Parietal lobe
Occipital lobe
Occipital lobe

977

Regions are matched between imaging and neuropathology on the basis of shared nomenclature and spatial overlap. The left column describes the anatomic sites from which the standard DIAN and Knight ADRC tissue blocks relevant to this study are taken, superimposed on a T1-weighted MR image of the FreeSurfer example participant "Bert". The right column depicts the parcellation and segmentation of "Bert" at the same levels. In reality, all tissue is sampled from the left hemisphere and all imaging measures are derived from the left hemisphere, but for convenience of representation, these regions are sometimes depicted on the contralateral hemisphere in the figure. In the nomenclature used for this study, the anatomic sites, with matched FreeSurfer (Desikan-Killiany atlas) regions in parenthesis, are: anterior cingulate (caudal anterior cingulate); caudate (caudate); cerebellum (cerebellar cortex); frontal lobe (rostral middle frontal); parietal lobe (inferior parietal); pons (brainstem); posterior cingulate (posterior cingulate); putamen (putamen); temporal lobe (middle temporal); amygdala (amygdala); entorhinal cortex (entorhinal); globus pallidus (pallidum); hippocampus (hippocampus); occipital lobe (pericalcarine); parahippocampal gyrus (parahippocampal); thalamus (thalamus).

Online Resource 2 Exact ADAD mutations of the *PSEN1* gene investigated in this study

PSEN1 deletion intron 4
PSEN1 Asn135Ser
PSEN1 Asn135Tyr
PSEN1 Ile143Thr
PSEN1 Met146Leu
PSEN1 His163Arg
PSEN1 Ser169Leu

PSEN1 Ser170Phe
PSEN1 Gly209Glu
PSEN1 Ile229Phe
PSEN1 Ile229Phe
PSEN1 Thr245Pro
PSEN1 Cys410Tyr
PSEN1 Ile439Val

994